



Tectono-Stratigraphic and Thermal Evolution of the Western Betic Flysch: Implications for the Geodynamics of South Iberian Margin and Alboran Domain

Maxime Daudet, Frédéric Moutherneau, Stéphanie Brichau, Ana Crespo-blanc,
Cécile Gautheron, Paul Angrand

► To cite this version:

Maxime Daudet, Frédéric Moutherneau, Stéphanie Brichau, Ana Crespo-blanc, Cécile Gautheron, et al.. Tectono-Stratigraphic and Thermal Evolution of the Western Betic Flysch: Implications for the Geodynamics of South Iberian Margin and Alboran Domain. *Tectonics*, 2020, 39 (7), 10.1029/2020TC006093 . hal-02942999

HAL Id: hal-02942999

<https://hal.science/hal-02942999v1>

Submitted on 15 Apr 2022

HAL is a multi-disciplinary open access archive for the deposit and dissemination of scientific research documents, whether they are published or not. The documents may come from teaching and research institutions in France or abroad, or from public or private research centers.

Copyright

L'archive ouverte pluridisciplinaire **HAL**, est destinée au dépôt et à la diffusion de documents scientifiques de niveau recherche, publiés ou non, émanant des établissements d'enseignement et de recherche français ou étrangers, des laboratoires publics ou privés.

Tectonics

RESEARCH ARTICLE

10.1029/2020TC006093

Special Section:

Tethyan Dynamics: From Rifting to Collision

Key Points:

- The Flysch Complex of the Western Betic have been deposited close to their current position on the Iberian paleomargin
- AFT-AHe double-dating indicates that the Flysch Complex recorded fast heating/burial and cooling/exhumation between 20 and 15 Ma
- Tectono-thermal evolution of the flysch deposits is consistent with proto-Betic collision at ca. 50 Ma

Correspondence to:

F. Moutherau,
frederic.moutherau@get.omp.eu

Citation:

Daudet, M., Moutherau, F., Brichau, S., Crespo-Blanc, A., Gautheron, C., & Angrand, P. (2020). Tectono-stratigraphic and thermal evolution of the western Betic flysch: Implications for the geodynamics of South Iberian margin and Alboran domain. *Tectonics*, 39, e2020TC006093. <https://doi.org/10.1029/2020TC006093>

Received 26 FEB 2020

Accepted 31 MAY 2020

Accepted article online 12 JUN 2020

Tectono-Stratigraphic and Thermal Evolution of the Western Betic Flysch: Implications for the Geodynamics of South Iberian Margin and Alboran Domain

Maxime Daudet¹, Frédéric Moutherau¹ , Stéphanie Brichau¹ , Ana Crespo-Blanc² , Cécile Gautheron³ , and Paul Angrand¹ 

¹Geosciences Environnement Toulouse (GET), Université de Toulouse, UPS, Université Paul Sabatier, CNRS, IRD, Toulouse, France, ²Departamento de Geodinámica, Facultad de Ciencias, Universidad de Granada, Granada, Spain,

³GEOPS, University Paris-Sud, CNRS, Université Paris-Saclay, Orsay, France

Abstract The Betic-Rif orogen is a key region to understand the evolution of the plate boundary between Africa and Iberia/Europe. This study focuses on the Flysch Complex, which is considered the sedimentary cover of a domain originally positioned between the Iberian and Alboran margins. Based on stratigraphic and depositional evolution constraints, evidence for salt tectonics, combined with new apatite fission-tracks (AFT) and (U-Th-Sm)/He ages from the Flysch Complex and the Subbetic Zone, we propose a geodynamic interpretation for the formation of the Betic Cordillera, accounting for moderate N-directed transport of the Flysch Complex and synchronous exhumation between External and Internal Zones of the Betic. Early contraction between Africa and Iberia/Europe is reflected in the Cretaceous Flysch basin by a prolonged period of residence in the partial annealing zone for AFT and onset of foreland subsidence at 50 Ma. This stage lasted until the Early to Middle Miocene (20–15 Ma), marked by the rapid succession, in less than 5 Ma, of the deposition of Cenozoic flysch and their rapid exhumation. This event is interpreted to reflect the W-directed retreating mantle delamination between Africa and Iberia margins at the origin of the collapse of the proto-Betic orogenic domain and formation of the Alboran domain.

1. Introduction

The Betic Cordillera of southern Spain is understood to result from the subduction of the western Tethys since at the last the Eocene and collision of the Alboran domain with the South Iberian paleomargin (Figure 1; Chalouan et al., 2006; Crespo-Blanc & de Lamotte, 2006; Faccenna et al., 2001; Michard et al., 2008; Platt, Allerton, et al., 2003; Rosenbaum et al., 2002). Geodynamic interpretations of the area vary in terms of timing and nature of the deformational events, paleogeography of the tectonic units, and amount and veracity of subduction (Lonergan & White, 1997; Rosenbaum et al., 2002; Vergés & Fernández, 2012; see discussion in van Hinsbergen et al., 2014). Most contributions to the debatable geodynamic reconstructions of the subduction are from studies on the timing of metamorphism and exhumation of the Internal Zones (Augier et al., 2005; Booth-Rea et al., 2002; Goffe et al., 1989; Gómez-Pugnaire & Fernández-Soler, 1987; Platt et al., 2006, 2013; Vissers et al., 1995).

The western Betic exposes a series of siliciclastic deposits collectively referred as the Flysch Complex that can be followed almost continuously across the Gibraltar Arc and farther in the W-Mediterranean from the Rif to the Apennines (Crespo-Blanc & Campos, 2001; Guerrera et al., 1992; Martín-Algarra, 1987; Wildi, 1983). The Flysch Complex is interpreted as a thrust-imbricate resulting from the westward migration of shortening into the Iberian margin in the early Miocene (Luján et al., 2006). The commonly accepted allochthony of the Flysch Complex (Luján et al., 2006) with respect to the Iberian margin has been so far an assumption for the reconstruction of the spatial and temporal evolution of the western Mediterranean. The lack of constraints on the timing of exhumation and the nature of tectonic contacts however challenges the hypothesis of large tectonic movement of the Flysch Complex.

We first review the stratigraphy and basin evolution established for the external domains and the flysch series and reexamine the structural evidence in support of large thrust movement in the western Betic. We then

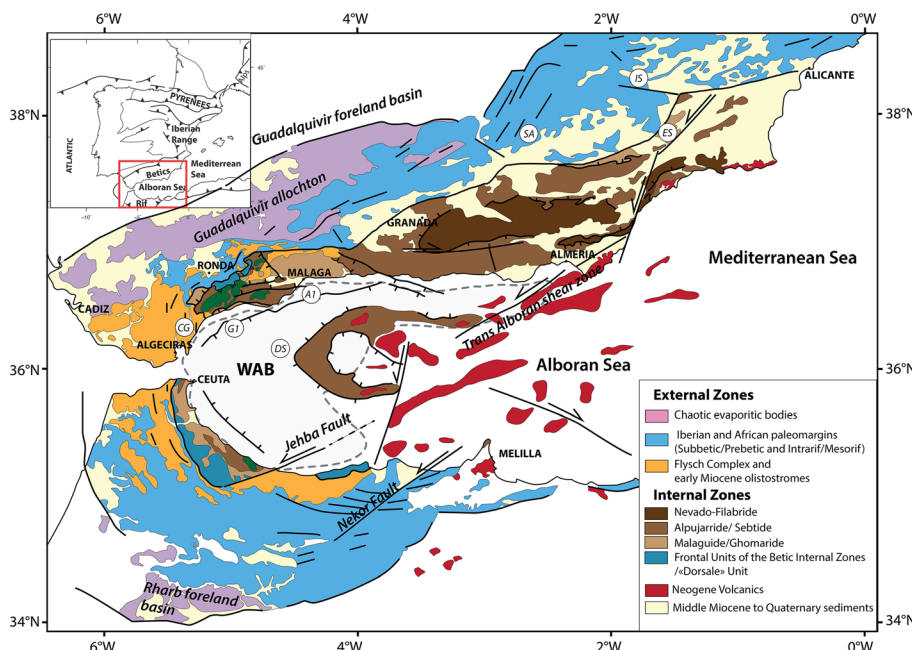


Figure 1. Geological map of the Betic and Rif Cordilleras (modified after Comas et al., 1999; Frasca et al., 2015). WAB = West Alboran Basin. Labeled white circles are wells and stratigraphic log discussed in the text and plotted on Figure 2 (CG = Cerro Gordo 1&2; G1 = Andalucía G1; A1 = Andalucía A1; DS: DSDP 121).

provide new apatite fission-track (AFT) and (U-Th-Sm)/He (AHe) ages from turbiditic sandstones of the Flysch Complex in the aim to document their thermal history.

2. Structure and Tectonic Evolution of the Internal Domains of the Betic

2.1. Geological Setting

The Betic-Rif domain is composed of several tectonic domains (Figure 1): (a) the Guadalquivir and the Gharb foreland basins; (b) the External Zones of the Betics and Rif; (c) the Flysch Complex; (d) the metamorphic complexes of the Internal Zones; and (e) the Alboran Sea basins, from the External toward the Internal Zones, respectively. The Internal Zones recorded a cyclical tectonic evolution marked by the following: (1) high-pressure during Variscan contraction followed by late Variscan partial melting (e.g., Sánchez-Navas et al., 2014, 2017; Zeck & Whitehouse, 2002); (2) rifting in the latest Permian-early Triassic (López-Gómez et al., 2019) and Jurassic magmatism and spreading in the Jurassic, as suggested by the ages of low-pressure protoliths of eclogite, pyroxenites, and amphibolite layers from the Alpujarride (AJ) Complex (Sánchez-Rodríguez & Gebauer, 2000; Tubía et al., 2009); (3) high-pressure metamorphism during Alpine nappe stacking followed by a regional Miocene extension and crustal thinning in the Alboran domain responsible for the LP-HT metamorphism event (e.g., Platt et al., 2013). The unmetamorphosed External Zones consist of three main zones, the Prebetic, only found in the eastern and central Betic; the Subbetic Zone forming the External Zones s.s.; and the Flysch Complex positioned between the Internal (Alboran) and External (European/Iberian) Zones. The Subbetic and Prebetic consist of Mesozoic to Tertiary sediments that were deposited on the variscan basement of the Iberian paleomargin (e.g., García-Hernández et al., 1980; Martín-Chivelet et al., 2002). The Flysch Complex is Cretaceous to Miocene deep-water sediments deposited in a basin probably floored by transitional or oceanic crust (Durand-Delga et al., 2000).

2.2. The Internal Zones and Alboran Sea Basin

2.2.1. Nappe Stacking in the Internal Zones

The Nevado-Filabride (NF) and AJ complexes (Figure 1) are made of paleozoic metasediments that preserve HP/LT mineral assemblages equilibrated mainly during earlier Alpine stages of convergence (Booth-Rea et al., 2002; Goffe et al., 1989; Gómez-Pugnaire & Fernández-Soler, 1987; Platt et al., 2006;

Vissers et al., 1995). In the NF complex, the HP/LT metamorphism (1.4–2 GPa, 600–690°C) is followed by LP-LT retrograde conditions (0.6–0.3 GPa, 600–300°C) (e.g., Augier et al., 2005; Gómez-Pugnaire et al., 2012). Geochronology (Rb-Sr, Lu-Hf, Ar-Ar, U-Pb) show ages for the HP metamorphism ranging between 60 and 17 Ma (Augier et al., 2005; Gómez-Pugnaire et al., 2012; Kirchner et al., 2016; Monié et al., 1991; Platt et al., 2006; Puga et al., 2002; Sánchez-Vizcaíno et al., 2001). The AJ complex, which lies structurally above the NF, recorded lower peak HP-LT conditions (from 0.7–1.1 GPa, 400–580°C) around the middle Eocene (Augier et al., 2005; Platt et al., 2013). Low-temperature cooling ages indicate that both the NF and the AJ complexes cooled and exhumed rapidly to upper crustal levels between 22 and 18 Ma (e.g., Platt, Whitehouse, et al., 2003). Zircon fission-track data from the NF complex further document rapid cooling from 300–240°C to near-surface temperatures between 12 and 6 Ma (Johnson, 1997; Vázquez et al., 2011).

The Malaguide complex is structurally the highest tectonic nappe of the Internal Zones. It is composed of a Paleozoic sedimentary succession unconformably overlain by widespread Triassic, including redbeds and subordinate conglomerates (Esteban et al., 2017; Perri et al., 2013). Remnants of unmetamorphosed Jurassic and Cretaceous strata are represented by limestones. They pass upward into an alternation of carbonaceous sandstones, conglomerates, marls, and marly limestones of Paleocene age. The Eocene sequence is represented by Nummulites and Alveolines limestones overlying unconformably on the Jurassic or lower Cretaceous strata. Locally, in the Sierra Espuña the Eocene succession of the Malaguide cover is more than 3-km thick.

The Frontal Units of the Internal Zones (“Dorsale Calcaire” of Durand Delga & Foucault, 1967) is a Mesozoic-Paleogene tectono-stratigraphic zone that is only found in the western part of the Betic above the Flysch Complex and below the Internal Zones (Figure 1). This intermediate zone is considered to be the Mesozoic cover of the Malaguide complex (Didon et al., 1973; Durand-Delga, 1972). It is composed essentially of nonmetamorphosed Triassic carbonates except close to the contact with the Ronda (and equivalent) peridotite bodies.

2.2.2. Alboran Sea Basin

The deep crustal and lithospheric structure of the Gibraltar arc region comprises the Betic-Rif cordilleras and the Alboran Sea (Figures 1 and 2). As a result of the back-arc extension, the crustal thickness is 15–20 km in the Alboran Sea whereas it reaches 50–45 km beneath the western Betic and the Rif below which a slab is imaged down to depth of 600 km (Figure 2) (e.g., Mancilla et al., 2015; Palomeras et al., 2017; Thurner et al., 2014). The basement of the Alboran Sea basin is made of the same metamorphic Paleozoic rocks as the AJ complex. This basin is divided in three subbasins: the Western Alboran Basin (WAB), the East Alboran Basin (EAB), and the South Alboran Basin (SAB) (Comas et al., 1999). Sediment thickness reaches 8 to 10 km in the WAB where the oldest sediments are Burdigalian (Comas et al., 1999; Couto et al., 2016; Iribarren et al., 2009) and is only 2–3 km in the SAB and EAB where the oldest sediments are Serravallian (Martínez-García et al., 2017). The AJ rocks drilled at ODP site 976 show metamorphic rocks exhumed to the surface by 18–20 Ma, consistent with rapid cooling at ~21–17 Ma documented by geochronological constraints in the AJ complex onshore (Esteban et al., 2004; Monié et al., 1994; Platt, Argles, et al., 2003). Since the late Tortonian (9 Ma), the Alboran Sea is undergoing contraction (e.g., Comas et al., 1999; Martínez-García et al., 2017).

3. Basin Evolution and Stratigraphy of the External Domains and the Flysch Complex

3.1. Mesozoic and Cenozoic Stratigraphy of the External Betic and Flysch Complex

3.1.1. Triassic and Jurassic: Initial Rift Phase

Well data from the Betic external and Prebetic domains show that subsidence related to rifting on the south-Iberian margin started during the Late Permian/Early Triassic time, from 270 Ma to 200 Ma (Figure 3 and López-Gómez et al., 2019). In the western Betic, Triassic sedimentary rocks are exposed in the Guadalquivir accretionary wedge (GAW) and in the chaotic complexes of the central and western Betic (Figure 4). The Buntsandstein facies is absent in the Subbetic and the sequence is restricted to Muschelkalk and Keuper facies (Martínez-García et al., 2017; Pérez-Valera et al., 2017) at the origin of the diapiric structures (Flinch & Soto, 2017). A detrital, continental to coastal Triassic facies is observed in the Malaguide which contrasts with Alpine-type carbonate-dominated series of the AJ (Martín-Algarra, 1987; Ortí et al., 2017). The flysch of the Campo de Gibraltar (CpG) lacks a Jurassic substratum (Figure 4). The

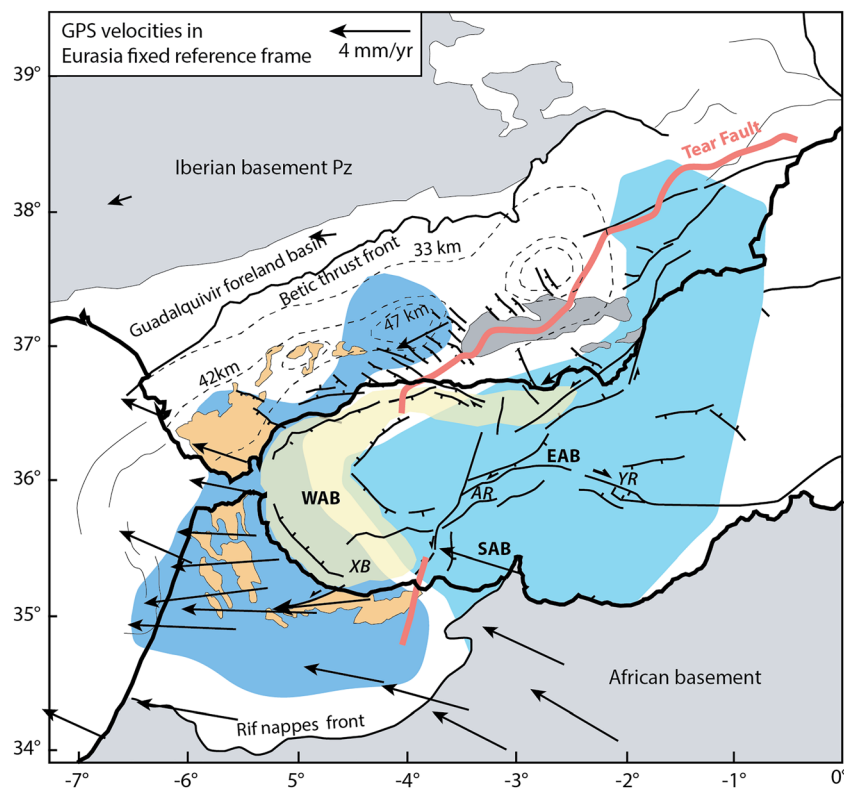


Figure 2. Main crustal features of the Betic and Alboran Sea and the Flysch Complex (orange). Arrows depict GPS velocities after Vernant et al. (2010). Moho depth variations beneath the Betic are based on Vs velocity and P-receiver functions from Mancilla et al. (2015) and Palomeras et al. (2017). Dark blue domain below the Gibraltar arc represents the domain of thick crust (40–50 km) and light blue domain represents the thinned crust (30–15 km) of the Alboran Sea (Palomeras et al., 2017). Position of the slab tear (thick red-line) is drawn after Mancilla et al. (2015). The Western Alboran Basin (WAB) depocenter is shown in light yellow. SAB and EAB are the South Alboran Basin and East Alboran Basin, respectively. YR, AR, and XB for Yusuf Ridge, Alboran Ridge, and Xauen Bank, respectively.

Camarote Unit, a transitional unit toward the Frontal Units of the Internal Zones, is made of Lower Cretaceous sediments and is interpreted to be originally attached, stratigraphically, to the Lowermost Cretaceous to latest Triassic succession of the Tajarillo Unit (Jabaloy-Sánchez et al., 2019; Olivier, 1984).

3.1.2. Early and Late Cretaceous: Second Phase of Rifting

A second phase of rift-related subsidence is recorded in the Betic from Late Jurassic (Bathonian, ~170 Ma) to Early Cretaceous (Albian, 100 Ma) for some wells (Figure 3, Hanne et al., 2003). The Early Cretaceous marks a change in the depositional system as revealed by the onset of siliciclastic influx forming the external flysch deposits of Northern Africa (Massylian and Mauretanian series of Wildi, 1983). On the Iberia margin, lower Cretaceous Boyar-Ubrique turbiditic formations are also found in the western Subbetic, and within the few outcrops of Mesozoic flysch of the Campo de Gibraltar (Figures 4 and 5). The Boyar flysch ranges from Berriasian to Maastrichtian and the Ubrique flysch from Albian to Maastrichtian (Bourgois & Chauve, 1971). The Ubrique flysch shows overturned limbs on the flanks of a diapiric structure made of Triassic evaporites that has reworked the initial contact with the Jurassic limestones, which is now lacking (see description in section 3). Isolated bodies of lower Cretaceous flysch are also found within the Flysch Complex like the Nogales and Camarote flysch (Didon, 1969). They are often found disconnected from the Tertiary cover (Figure 5), which makes their original position in paleogeographic reconstructions difficult to resolve.

3.1.3. Paleocene-Eocene: Onset of Foreland Subsidence and Collision

After a period of regression at the Cretaceous-Tertiary boundary, a regional transgression from the Danian (66–61 Ma), lower-middle Cuisian (Late Ypresian, 52–50 Ma), and middle Lutetian-Bartonian (45–38 Ma) is recorded in the Malaguide Complex. The acceleration of subsidence in the Malaguide Complex (Sierra Espuña) is most apparent from the middle Lutetian (45 Ma) (Figure 3). The most widespread

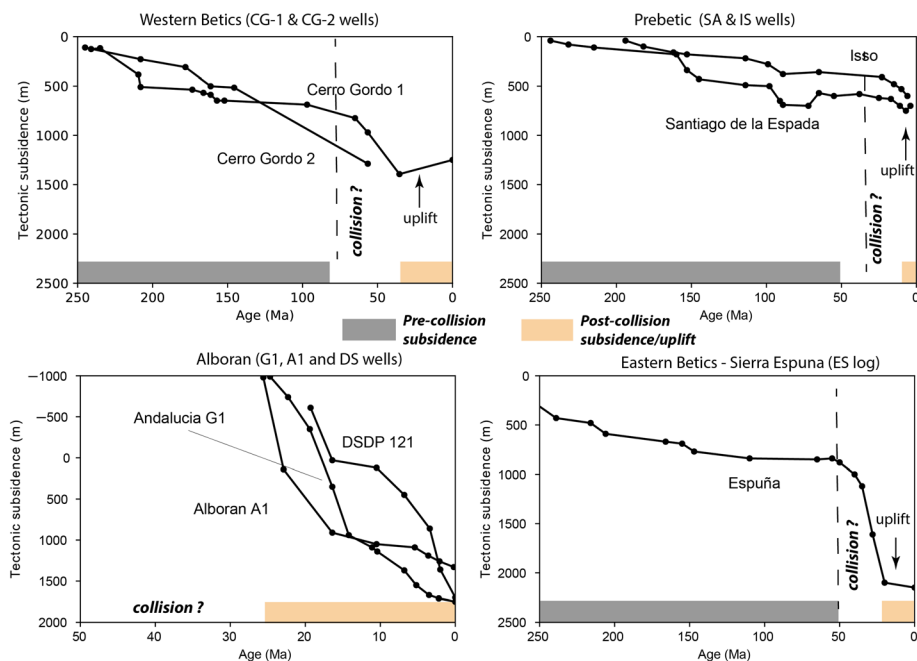


Figure 3. Subsidence evolution for some wells of the western Betic (left side) and eastern Betic, the pre-Betic (right side) and stratigraphic log (Espuña) of the Malaguide Complex after compilation of Hanne et al. (2003). See location on Figure 1. The gray domain depicts the timing of pre-collision subsidence (rift-related) while the light orange-filled domain shows the post-orogenic evolution defined by uplift onland and fast subsidence offshore (Alboran Sea) from about 20–25 Ma. In between, the collision is reflected by the onset of foreland subsidence (50 Ma for Espuña), a bit earlier in the western Betic (Late Cretaceous) or slightly later in the Prebetic (~40 Ma).

transgression is outlined by the deposition of 10–20 m of shallow-marine carbonaceous platform unconformably overlying the late Cretaceous deposits and established over all the Malaguide Complex from the Late Ypresian, 52–50 Ma (Hanne et al., 2003; Lonergan & Mange-Rajetzky, 1994; Maaté et al., 2000). Field data in the Prebetic also agree with a transgression in late Thanetian (56 Ma) to late Ypresian (50 Ma) as shown by the development of a turbiditic basin (Martín-Chivelet & Chacón, 2007) that they interpret to reflect the initiation of Africa-Europe convergence. This early stage subsidence is however much less clear from SA and IS wells that suggest an acceleration in the Eocene (Figure 3). We infer from the stratigraphy and subsidence analyses that foreland flexural subsidence, in the eastern Betic Cordillera and at the front of the Malaguide Complex, started in the lower Eocene (Late Ypresian, ~50 Ma), at the latest.

The Paleocene and the Eocene-Oligocene sedimentation in the Subbetic domain (Capas-Rojas Formation) is made of marls or shales interbedded with calcareous turbidites whereas Paleogene series of the Flysch Complex (Colorín and Benaíza Formations) show much more marly, carbonate rich, and much less deep facies (Figure 4) with some levels of conglomerates or breccias (Arguelles unit; Figure 4). In the Boyar-Ubrique and Alta Cadena regions, from the internmost part of the Median Subbetic trough, the Paleocene is characterized by the *Microcodium*-rich turbiditic limestones (Alcalá-García et al., 2002; Bourgois, 1978; Martín-Algarra, 1987) that attest for sediment influx from the continent and deposition on local slopes. The microcodium-rich turbidites are also documented, on top of the late Cretaceous sediments of the Malaguide complex. In the Malaguide Complex nearby Malaga city or in Sierra Espuña they appear in place encrusting Mesozoic limestones and continental Paleocene conglomerates. The Malaguide was most likely probably the source for redeposited Microcodium in the Frontal (e.g., Argüelles Fm.) and Flysch Complex units (Pers. Comm. Martín-Algarra). They are followed unconformably by Eocene calcareous turbidites with alveolines and numulites (Figure 4) (Guerrera et al., 2006; Maaté et al., 2000; Martín-Martín et al 1997; Serrano et al., 1995; Serra-Kiel et al., 1998) that witness the initiation of the foreland subsidence and therefore collision.

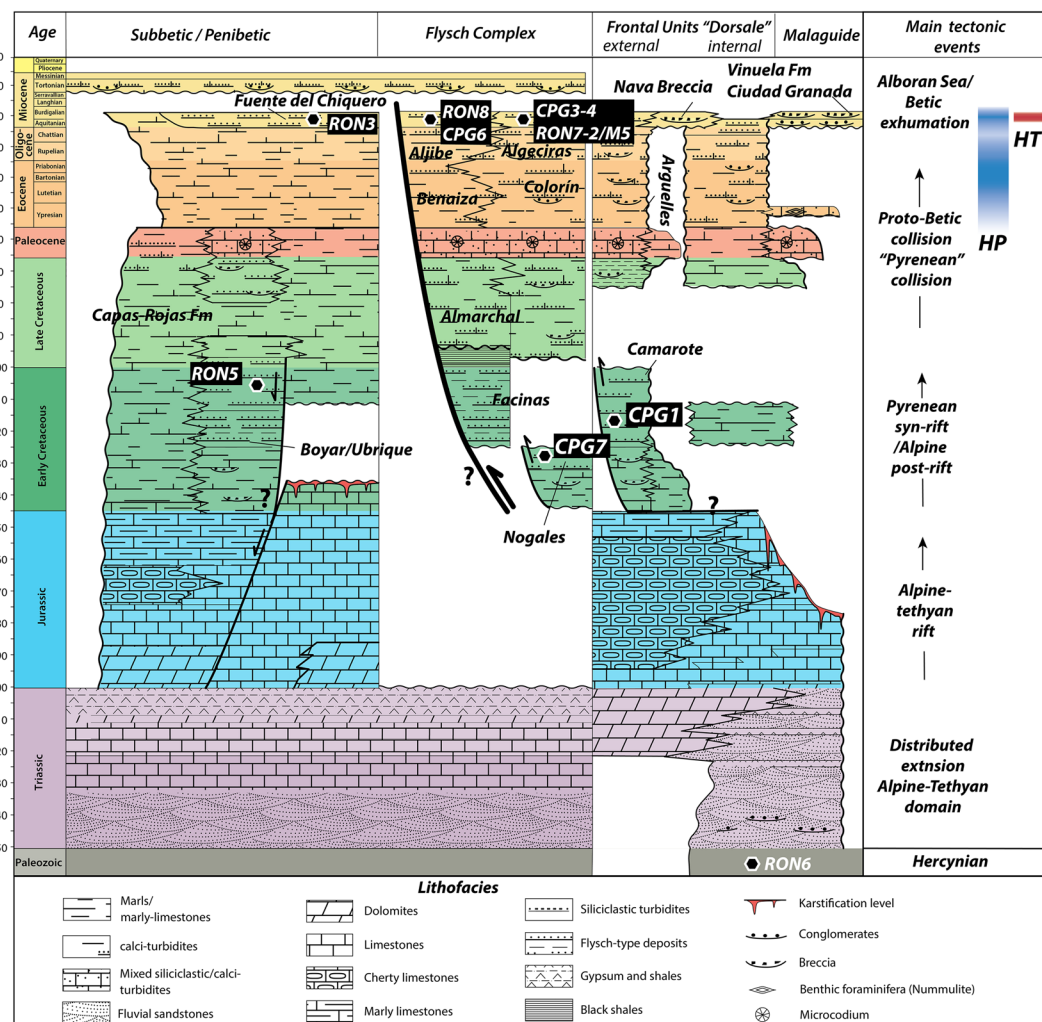


Figure 4. Mesozoic-Cenozoic stratigraphy of the Betic and main tectono-metamorphic events. The compilation was made after the works of Bourgois (1978), Martín-Algarra (1987), Martín-Algarra et al. (2009), and Vera et al. (2004) for the External Zones; Guerrero and Martín-Martín (2014) and Jabaloy-Sánchez et al., 2019 for the Flysch Complex; and Serrano et al. (1995, 2007), Serra-Kiel et al. (1998), Martín-Martín (1996), Maaté et al. (2000) for the Internal Zones. Question marks indicate alleged tectonic contacts between the Boyar-Ubrique flysch, the upper Triassic, and the Subbetic/Penibetic, and between Camarote flysch and the Frontal Units of the Internal Zones Jurassic substratum.

3.1.4. Oligocene-Miocene

Backstripping reconstructions show that rapid subsidence occurred in the Alboran Sea basin from the Early Miocene in response to crustal thinning of the metamorphic basement (i.e., 25–20 Ma on Figure 3; Hanne et al., 2003). Onshore, a nearly synchronous uplift (Western Subbetic) or a slight decrease in subsidence (Sierra Espuña) reflects the migration of thrust loads toward the North. The fast transition from subsidence to uplift in those domains is preserved along some sections of the internal domains. The Upper Oligocene-uppermost Aquitanian Ciudad Granada group (up to 20.5 Ma; Figure 3) postdates an early Alpine deformation stage but predates the main exhumation event of the Betic-Rif belt, which culminates in late Burdigalian (Crespo-Blanc & Campos, 2001; Martín-Algarra, 1987). The transgressive Burdigalian Viñuela group (Figure 3) found on top of the Ciudad Granada group unconformably overlies both the AJ and the Malagueide complexes. The clasts forming the detrital material of Viñuela group are sourced from the Malagueide and AJ basement, thus providing constraints on the timing of subaerial exhumation of the Internal Zones. Subsidence renewed during the Tortonian (10.4–8 Ma) in the Guadalquivir Basin and was followed by a regional post-shortening uplift. From the latest Oligocene to the early Miocene, sedimentation changed from carbonate-dominated to siliciclastic, which is outlined by the turbiditic sequences of the

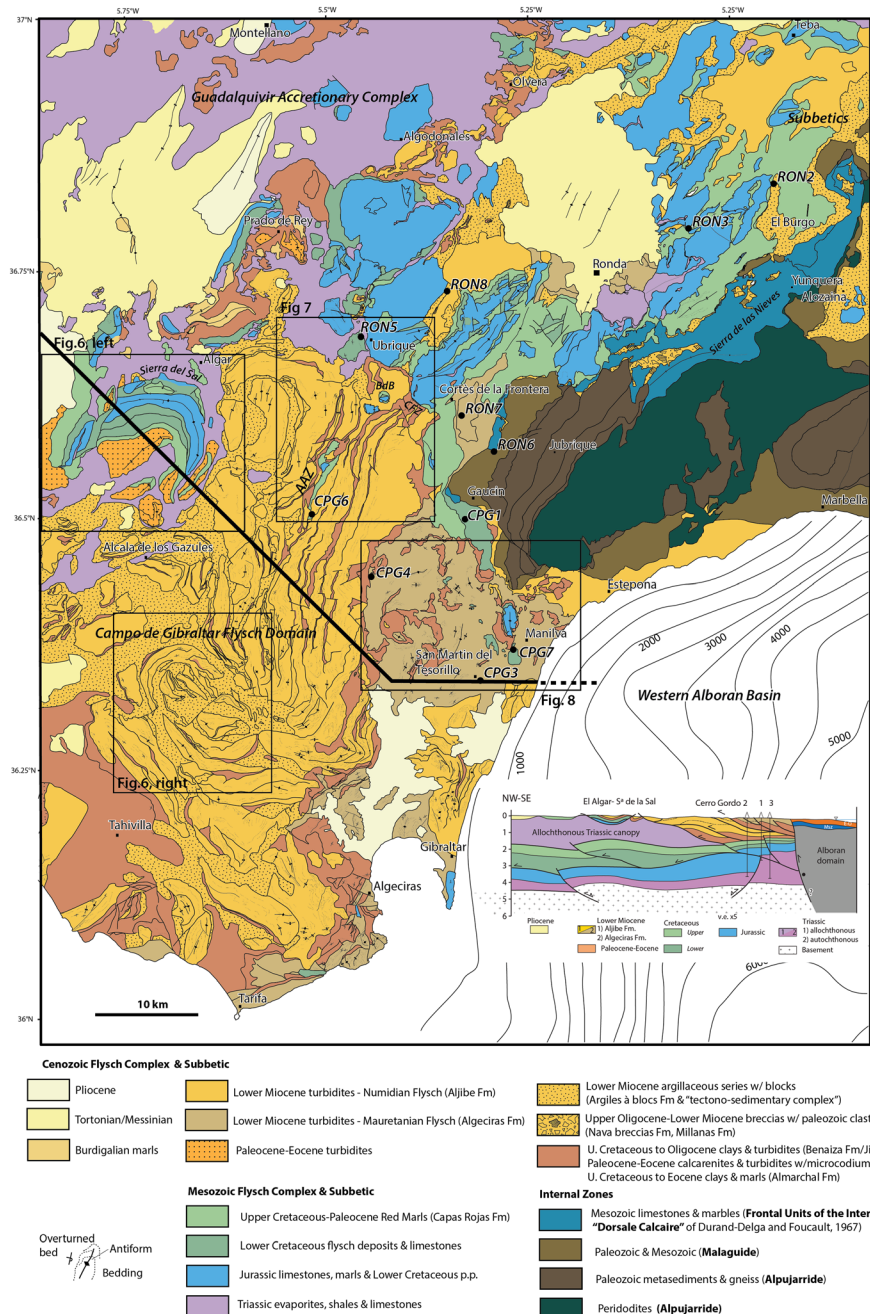


Figure 5. Detailed geological map of the studied area of the western Betic and division of lithological units in the Cenozoic Flysch Complex and Subbetic drawn after a compilation of the 1:50000 maps of Spain and the stratigraphic correlation shown in Figure 4. Cross-section (location shown as black thick line) is slightly modified after Flinch and Soto (2017). Main tectono-stratigraphic domains onland and isobaths for the Western Alboran Basin are shown. Black circles depict samples used for AHe and AFT analyses. Insets show location of Figures 6, 7, and 8. AAZ = Arnao Accommodation Zone; PdB = Peñón del Berrueco; CFZ = Colmenar Fault Zone. Geological maps are available at <http://info.igme.es/cartografiadigital/geologica/Magna50>.

Algeciras and Aljibe formations (Didon, 1969; Guerrera et al., 1992; Hoyez, 1989; Martín-Algarra, 1987). Miocene turbidites are also found above gypsum/clay Triassic layers, or in stratigraphic contact with the late Cretaceous to Paleogene sediments of the Subbetic in the region of Peñón-Grande and Cortes de la Frontera (Figure 5). In the absence of more precise petrographic description, we correlate these subbetic Miocene turbiditic deposits with the turbiditic sequences of the Flysch Complex.

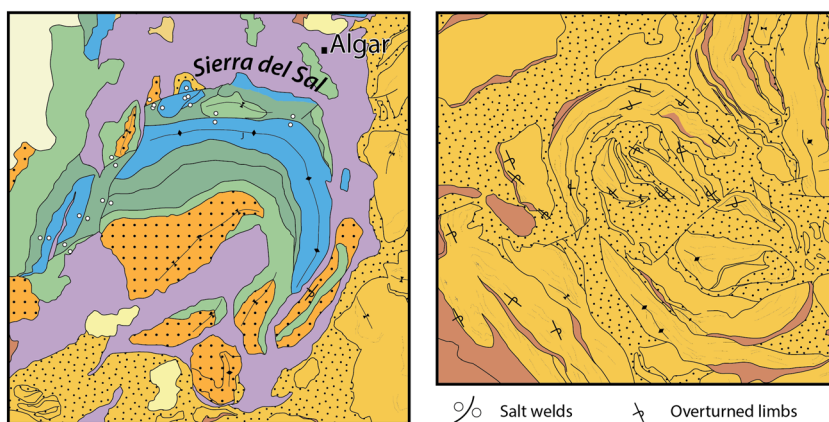


Figure 6. Extracts of Figure 5 showing horseshoe structures and salt welds as documented in the Campo de Gibraltar flysch, near Alcalá de los Gazules. They reveal flank rotations and vertical-axis rotation induced by salt movement, and salt welds reflect salt removal.

In summary, stratigraphic constraints suggest that the Betic recorded a pre-Miocene orogenic event at about 50 Ma outlined by subsidence and transgressive sequence in the Malaguide (Figure 3). The good correlation between Mesozoic-Cenozoic deposits of the Flysch Complex and those of the Subbetic area (Figure 4), despite deeper facies are found in the Flysch Complex, suggests these domains could originally be part of the same basin.

4. Structural Position of the Flysch Complex

4.1. Salt Tectonic Features in the Flysch Complex

Salt tectonics is known to be at the origin of several peculiar structural features observed in the western Betic (Flinch & Soto, 2017). The GAW represents an accretionary complex emplaced during the Miocene, from late Burdigalian to Tortonian, made of the Median and External Subbetic Zones and the Flysch Complex glided northward and emplaced in the Guadalquivir Basin (Pérez-Valera et al., 2017). It is made of a chaotic mélange comprising blocks of Meso-Cenozoic sediments in a matrix of Triassic clays and gypsum. The apparent structural complexity of the GAW reflects diapiric events that occurred first on the Iberian paleo-margin between late Cretaceous and Paleocene. These initial phase of salt mobilization was followed by the extrusion and spreading of salt sheets associated with north-propagating frontal thrust during the late Oligocene to early Miocene (Berástegui et al., 1998; Flinch et al., 1996; Flinch & Soto, 2017; Pérez-Valera et al., 2017; Vera, 2000). The dominant control by salt on the tectonics of the Subbetic is further indicated by (1) Triassic evaporites found resedimented in the Cretaceous-Paleocene, (2) the lack of Jurassic or lower Cretaceous strata that are otherwise present in the Subbetic, and (3) the identification of Cretaceous-Paleogene subbasins (Flinch & Soto, 2017). These authors eventually identified a 60 km-large allochthonous Triassic salt canopy at the front of the Subbetic (section 1).

Salt tectonics is also a dominant process in CpG and Sierra de Cadiz area (Figure 5). From Prado del Rey in the N, through Alcalá de los Gazules, Tahivila in the center down south to Tarifa, the Cenozoic sandstone layers of the Flysch Complex exhibit vertical to overturned limbs, sharp and discordant contacts. The elongated folds of CpG commonly form contorted features, or very characteristic horseshoe structures, indicating rotations induced by salt movement (Figure 6). In the region of Alcalá de los Gazules, salt diapirs pierce the carapace of the salt canopy made of flysch sediments. South of Algar, the Sierra de la Sal form a 6-km large horseshoe structure made of Jurassic-to-Paleogene succession, with a number of welds that reflects salt removal (Figure 6). Other structures like the Arnao Accommodation Zone (AAZ of Luján et al., 2006; Figure 7) made of isolated outcrops of flysch and subbetic limestones, surrounded by opposite vergent folding of the flysch, document a salt suture (e.g., Jackson & Hudec, 2017). Between most of the folds of CpG, a tectono-sedimentary mélange made of Miocene shale matrix mixed with blocks of Jurassic, Cretaceous, and Paleogene as well as Miocene turbiditic sandy deposits support the presence of salt pillows, upwellings, as well as mud diapirism below the Flysch Complex. Below the salt canopy, exploration well data and

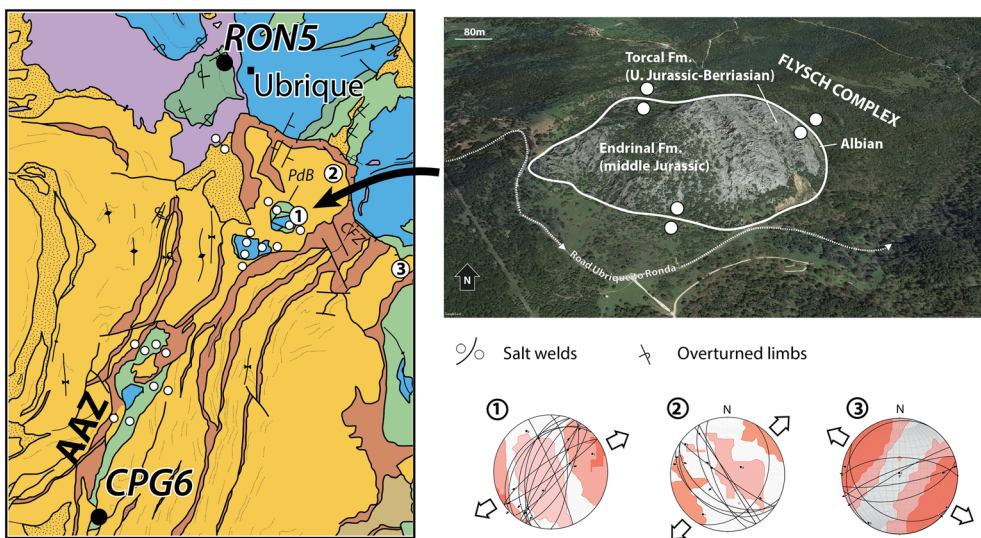


Figure 7. Field example of a salt weld in the Flysch Complex that juxtaposed Jurassic limestone (blue) with the Cenozoic Aljibe Formation, near Ubrique at the Peñon del Berrueco (PdB). Jurassic is interpreted as remnants of the carapace associated with emplacement of the salt canopy. Stereoplots showing fault-slip data and inferred direction of extension in the Ubrique area are also shown. CFZ (Colmenar fault zone) and AAZ (Arnao Accommodation Zone).

seismic reflection lines show a complete subbetic stratigraphic section overlying autochthonous Triassic evaporites (Flinch & Soto, 2017).

4.2. Contact Between Flysch Complex and the Subbetic Series

Given the importance of salt tectonics in the western Betic, one major issue was to correlate between the dismembered units of the flysch series. The contact of Cenozoic sandy turbidites of the Flysch Complex with the adjacent subbetic series is generally poorly preserved. Where it can be observed, the contact is characterized by diffuse small scale high-angle normal faults and strike-slip faults compatible with a ESE-WNW direction of extension in the region of Ubrique to N-S extension in the region of Estepona (Figures 7 and 8). These normal faults often delineate the contact between the Upper Cretaceous “Capas Rojas” (Figure 4) of the Subbetic and the flysch, which reflects the mechanical stratigraphy between weak red marly limestones and thicker, more competent flysch series. We focused our investigation along the road from Ubrique to Cortes de la Frontera and near El Burgo on the road from El-Burgo to Ronda (Figure 5). Isolated mesozoic block from the Subbetic/Penibetic found within the flysch of CpG have been interpreted as tectonic windows, thus supposedly attesting for the allochthonous character of the Flysch Complex (Crespo-Blanc & de

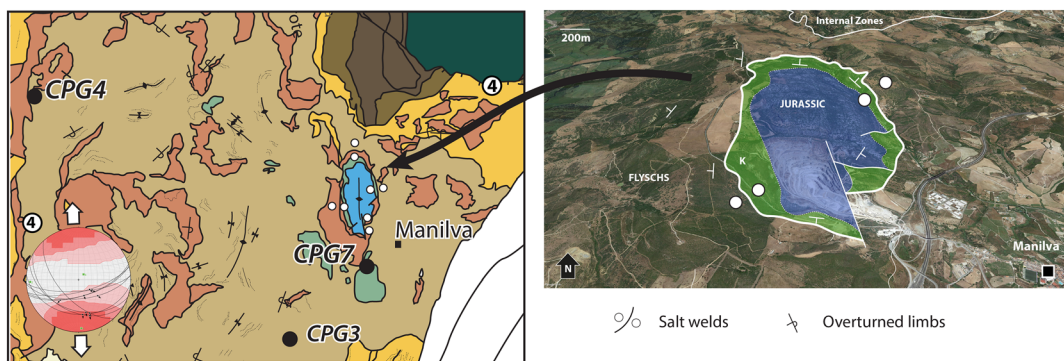


Figure 8. Field example of salt weld in the Flysch Complex between Jurassic (blue)/Cretaceous (green) carbonates and the Algeciras Formation, exposed close to Manilva. This is another example together with Figure 7 of the carapace. Stereoplots showing fault-slip data and inferred direction of extension south of the Ronda massif at the contact between the peridotites and the flysch series.

Lamotte, 2006; Luján et al., 2006). Similar outcrops of subbetic limestones can be found in different localities, along the AAZ and NW of Manilva. Near Manilva, the Peñón Del Berrueco (Figure 7), at the northern tip of the AAZ, shows a condensed section of folded Jurassic and Upper Cretaceous limestones surrounded by the Flysch Complex. Here the Upper Cretaceous “Capas Rojas” Formation is cut by steeply dipping dextral normal faults oriented NNE-SSW oblique to the bedding and to the contact with Flysch Complex. We interpret this structure as a remnant of the carapace of mezozoic rocks resting on top the Triassic allochthonous salt. The lack of significant tectonic movement along the main contact suggests the flysch succession are in a normal stratigraphic position above the older Upper Cretaceous red marls. The Manilva outcrop to the south shows a similar feature (Figure 8). Taken together, field observations indicate the contact between the Flysch Complex and the Subbetic is an original stratigraphic contact that has been reworked by salt movements and additional bedding-parallel shear.

4.3. Contact Between Flysch Complex and Internal Zones: The Tecto-Sedimentary Mélange

An enigmatic chaotic formation is exposed at the front of the Internal Zones, in the CpG area, and overlies unconformably the Malaguide and AJ in the region of Alozaina (south of Yunquera and El Burgo; Figure 5). This formation has been given different names, including the “Argiles à blocs” formation laterally defined as Neonumidian (AaB; Bourgois, 1978), tecto-sedimentary complex (Peyre, 1974), Numidoide and Argillas Variegadas (Martín-Algarra, 1987), or La Joya Olistostomic Complex (Suades & Crespo-Blanc, 2013) in the region of Alozaina. The sediment matrix is Burdigalian based on the youngest resedimented foraminifera (Bourgois, 1978; Feinberg & Olivier, 1983; Martín-Algarra, 1987; Peyre, 1974) and could even reach Serravallian to Langhian in Alozaina (Suades & Crespo-Blanc, 2013). The formation contains meter-to-kilometer-scale blocks, among which are found some Triassic sandstones, clays, and evaporites but more generally Jurassic and Cretaceous limestones and marly limestones from the Subbetic, Paleocene to lower Miocene marls, and the turbiditic sandstones of the Flysch Complex. The relationships with salt movement in the AaB are suggested by the highly deformed layers of Triassic evaporites in contact with overturned and disconnected layers of turbiditic sandstones of the Flysch Complex. We suggest the AaB is a collapsed carapace made of Mesozoic-Cenozoic cover formed on the slopes of a N-migrating escarpment of an allochthonous salt sheet, analogous to salt-related frontal compressional structures described in the Gulf of Mexico (Jackson & Hudec, 2017).

In summary, taking into account the important role played by salt tectonics, we infer that many if not all the geological contacts between the Flysch Complex and underlying rocks may be explained by salt tectonics. This, together with the lack of evidence for thrusting relationships between the Flysch Complex and Subbetic/Penibetic and the first-order stratigraphic correlation (Figure 4), despite the flysch series are defined by deeper facies than the Subbetic units, lead us to propose that the Flysch Complex was deposited in deeper environment of the Iberian paleomargin.

5. Low-Temperature Thermochronology

5.1. Samples Description

Twelve sandstones have been collected in lower Cretaceous and lower Miocene turbiditic sandstones of the Flysch Complex for AFT and (U-Th)/He analyses (Figure 9). These two thermochronological systems were preferred because they are most likely to be reset, considering the thickness of the flysch series of 1–2 km (Cerro Gordo wells of Figures 3 and 5; Flinch & Soto, 2017). Sampling was made to examine whether the Flysch Complex exhumed as a coherent unit on a regional scale by (1) exploring the maximum burial depths, (2) providing first-order comparison of thermal histories within the flysch series, currently exposed in different structural settings (CpG and AaB), and for different periods of deposition (Mesozoic and Cenozoic). All of our samples were collected between sea level and about 1 km (Table 1). Because AFT and AHe thermochronologic systems are characterized by closure temperatures between 110 and 70°C (3.6–2.3 km for 30°C/km), samples elevation is expected to have only minor impact, if any, on their time-temperature histories.

Samples RON8 and CPG6 were collected from the same Aljibe formation (Figures 4 and 9), close to the contact with the underlying late Cretaceous-Paleogene red marly limestones of the Subbetic. CPG6 belongs to the CpG area whereas RON8 is sampled from a sandstone body of Aljibe unit embedded in the “Argiles à Blocs” (AaB) formation according to the IGME map of Ubrique (Figure 4). CPG3, CPG4 and RON2,

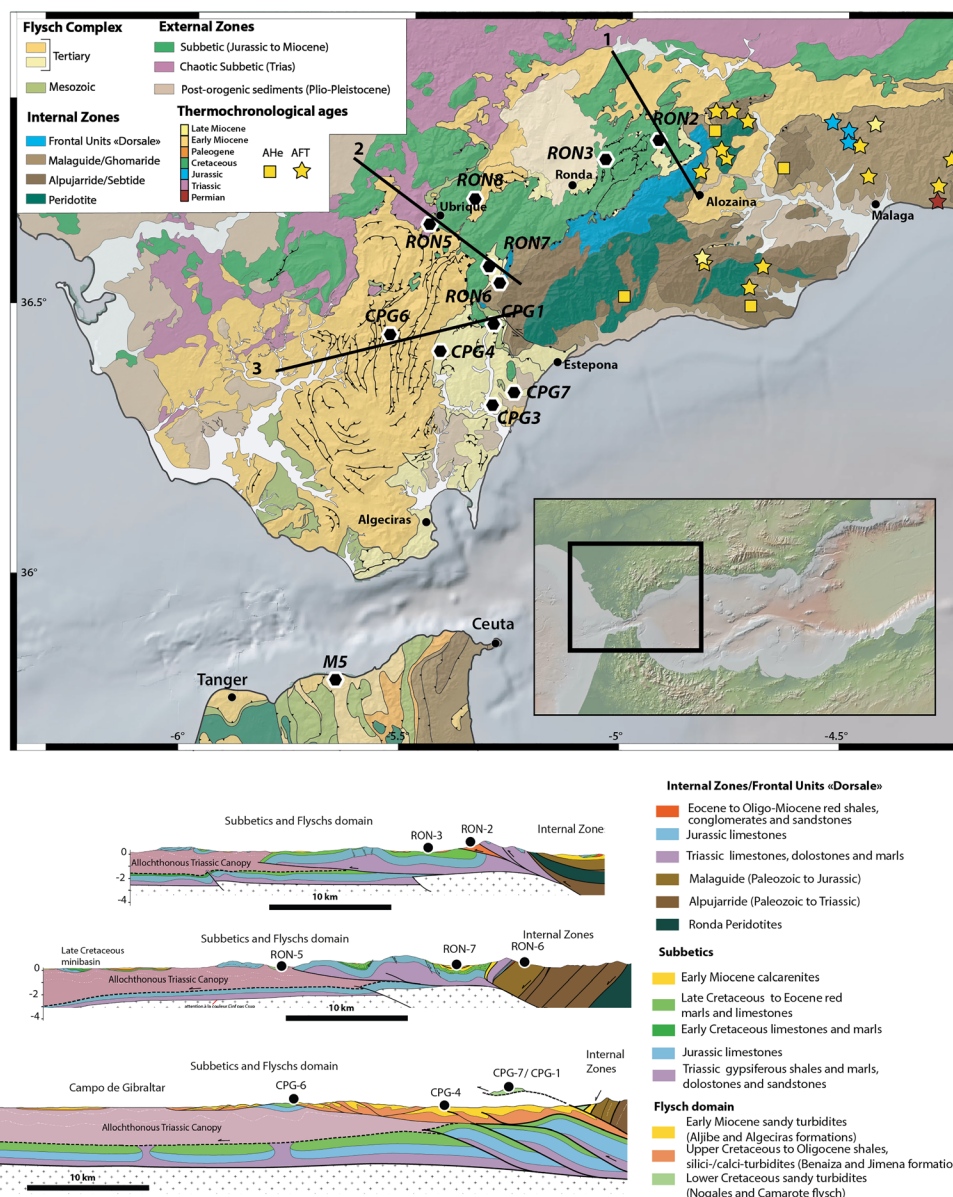


Figure 9. (top) Simplified geological map of the external part of the western Betic and location of collected samples. We color-coded cooling AFT and AHe ages in the internal metamorphic domains after Frasca et al. (2015) for AHe and AFT data compiled after Platt, Argles, et al. (2003) and Esteban et al. (2004). (bottom) Geological cross-sections of the western Betic proposed to illustrate the structural position of our samples in the Flysch Complex. Structural constraints in the External Zones are mainly from geological maps complemented by our own field survey. Structure of the Internal Zones are from work Frasca et al. (2015) in the east and Flinch and Soto (2017) in the west.

RON7 were sampled from the Algeciras formation, and M5 from the Beni-Ider formation, its Rifian equivalent (Figures 4 and 9). CPG4 and CPG3 sandstones are from Campo de Gibraltar and RON7, RON2 samples were sampled from the AaB formation as isolated sandstones from the same Algeciras formation (Figures 4 and 9). Remnants of the Cretaceous flysch exposed in the Betic were also collected. They include CPG7 and CPG1 from the Nogales and Camarote flysch that correspond to the Mauretanian and Predorsalian Cretaceous turbiditic sandstones. Sample RON5 was collected in late Albian Ubrique turbidites, a narrow sedimentary system deposited on the Iberian paleomargin (Figure 4). RON3 are turbiditic sandstones in Penibetic position (Aquitanian-Burdigalian Fuente del Chiquero Formation; Martín-Algarra, 1987) in a structural position equivalent to that of the Algeciras Formation RON7, RON2

Table 1
Apatite Fission Track Age Data for the 12 Analyzed Samples

Name	Lat	Lon	Alt.	Formation	Age	Nb	$\rho d^{(a)}$	ρs	ρi
						(Nd)	(Ns)	(Ni)	
CPG3	36°20'18.96"N	5°18'5.79"W	50	Algeciras	Early Miocene	13	1.65 [14622]	0.51 [59]	2.60 [314]
CPG4	36°26'33.79"N	5°26'33.48"W	60	Algeciras	Early Miocene	30	1.61 [14771]	0.61 [204]	2.96 [1003]
RON2	36°49'24.65"N	4°56'54.79"W	675	Algeciras	Early Miocene	27	1.64 [14771]	0.12 [333]	3.40 [1713]
RON7	36°35'54.26"N	5°19'56.94"W	360	Algeciras	Early Miocene	35	1.68 [14822]	0.11 [425]	4.69 [2002]
M5	35°49'56.72"N	5°36'56.33"W	0	Beni-Ider	Early Miocene	51	1.43 [12719]	0.13 [1092]	4.40 [3822]
CPG1	36°29'49.76"N	5°19'26.29"W	320	Camarote	Early Cretaceous	31	1.75 [6205]	0.21 [38]	2.52 [815]
CPG7	36°22'29.93"N	5°15'54.13"W	161	Nogales	Early Cretaceous	37	1.67 [14771]	0.16 [600]	2.10 [776]
RON8	36°42'47.55"N	5°22'3.83"W	860	Aljibe	Early Miocene	2	1.67 [14822]	0.21 [103]	3.74 [187]
RON6	36°33'56.65"N	5°17'38.03"W	790	Malagueña	Carboniferous	11	1.69 [14822]	0.34 [30]	1.74 [152]
RON5	36°40'37.89"N	5°27'12.50"W	420	Ubrique	Mid-Cretaceous	21	1.70 [14822]	0.51 [233]	4.88 [2102]
RON3	36°47'25.52"N	5°3'2.25"W	1,150	Fuente del Chiquero	Early Miocene	21	1.71 [14822]	0.91 [217]	4.48 [1105]

Note. Samples location, approximate elevation, formation, and stratigraphic ages. In italic samples that were not used for thermal modeling. Nb = number of counted grains, ρs , ρi : respectively, spontaneous and induced, track density; ρd = induced track density in the external detector (CN5); RE = age dispersion; $P\chi^2$ = probability of obtaining χ^2 value for Nb degrees of freedom; STD = standard deviation.

Table 1
Continued

Name	RE (%)	P _{X2} (%)	U (ppm)	Central age (Ma $\pm 1\sigma$)	Track length (μm)	Std (µm)	Nb confined tracks	Populations
CPG3	17.5	24.27	19.71	43.3 \pm 6.6	11.6 \pm 0.66	1.29	2	-
CPG4	58.5	0.00	21.46	51.8 \pm 7.1	6.905 \pm 0.66	3.00	4	P1:26.4 \pm 3.5 Ma P2:9.8 \pm 1.2 Ma
RON2	81.6	0.00	25.93	57.8 \pm 10.3	9.71 \pm 0.66	2.28	32	P1:39.5 \pm 3.9 Ma P2: 166 \pm 17 Ma
RON7	66.2	0.00	35.02	47.9 \pm 4.0	12.41 \pm 0.66	2.43	9	P1:40.9 \pm 3.2 Ma P2:151 \pm 31 Ma
M5	62.8	0.00	38.41	57.5 \pm 5.7	10.99 \pm 0.66	1.97	81	P1:40.9 \pm 2.2 Ma P2:129 \pm 9.4 Ma
CPG1	40.1	0.00	17.96	231.0 \pm 30.4	11.23 \pm 0.66	1.82	14	P1: 153 \pm 14 Ma P2: 289 \pm 37 Ma
CPG7	35.3	0.03	15.70	157.7 \pm 21.6	9.547 \pm 0.66	1.95	14	P1: 134 \pm 12 Ma P2:264 \pm 30 Ma
RON8	13.5	5.78	28.08	134.7 \pm 22	8.03 \pm 0.66	2.18	12	-
RON6	13.5	22.90	12.89	46.6 \pm 9.6	-	-	-	-
RON5	14.6	8.71	35.90	26.2 \pm 2.1	10.45 \pm 0.66	2.59	22	-
RON3	70.1	0.00	32.80	43.7 \pm 7.8	10.36 \pm 0.66	3.38	15	P1:36.8 \pm 3.7 Ma P2:113 \pm 21 Ma

Note: Samples location, approximate elevation, formation, and stratigraphic ages. In italic samples that were not used for thermal modeling. Nb = number of counted grains, ρ_{s} ; i: respectively, spontaneous and induced, track density; pd = induced track density in the external detector (CN5); RE = age dispersion; $P\chi^2$ = probability of obtaining χ^2 value for Nb degrees of freedom; Std = standard deviation.

and CPG6. We also collected RON6 sample in a Devono-Carboniferous mica-rich sandy turbidites from the Malaguide complex.

5.2. AFT and (U-Th)/He Analyses and Thermal Modeling

Samples were prepared for AFT analyses at the GET laboratory in Toulouse. Apatite grains were separated from approximately 7 kg bulk samples, such quantities being necessary for detrital low temperature thermochronology. After crushing and sieving, the $<500\text{ }\mu\text{m}$ fraction was first roughly separated with a shaking table. Then we performed density separation using heavy liquids to separate the apatites ($2.9 < \rho < 3.3$) from the zircons ($\rho > 3.3$). Finally, magnetic separation was achieved with a Frantz to obtain a clean enough fraction, ready to be mounted in epoxy resin. Spontaneous tracks were revealed through polishing of grain mounts and etching with 5-N HNO_3 at 21°C for 20s. Capsules containing the mounted samples were irradiated with thermal neutrons at the FRM II in Garching, Germany. Standard glass CN-5 was used as a dosimeter to measure the neutron fluence decrease through the capsule. After irradiation, induced fission tracks in the external detectors (low-U muscovite) were etched in 40% HF at 21°C for 40 min. AFT central ages ($\pm 1\sigma$) (Galbraith & Laslett, 1993) were measured and calculated using the zeta calibration methods with International Union of Geological Sciences age standards (Hurford & Green, 1983).

Handpicking of apatite crystals, in order to select inclusion-free crystal, was carried out in the GET laboratory. We calculated the FT ejection factors using the procedure of Gautheron and Tassan-Got (2010) and Ketcham et al. (2011). Crystal dimension and geometry were measured along two axes, considering the apatite crystals as regular hexagonal prisms, grains had in general a minimum width of $60\text{ }\mu\text{m}$ to minimize the effect of alpha particles ejection. Error on FT factor was propagated to AHe ages using Ehlers and Farley (2003) formulae. AHe analyses were carried out at the GEOPS laboratory (Université Paris-Sud, France and analytical details can be found in Fillon et al., 2013). He, U, Th, and Sm extraction and measurement follow the protocol described in Recanati et al. (2019). In addition, the apatite crystal weight was calculated using the Ca content determined with isotopic dilution using ^{42}Ca spike.

To bring constraints on the thermal histories of our samples, we perform joint-inversion modeling of AFT and AHe data on double-dated samples using software QTQt (Gallagher, 2012). QTQt takes into account the multikinetic AFT annealing model of Ketcham et al. (2007), distribution of track lengths and composition of apatite grains (Dpar). For AHe, QTQt incorporates recent kinetic models for helium diffusion in apatites (Flowers et al., 2009; Gautheron et al., 2009). These two diffusion models may produce different results, depending on the integrated thermal history of each grain. The inversion procedure uses a Bayesian “Markov chain Monte Carlo” algorithm to determine the best time-temperature path reproducing our data through a large number ($>200,000$) of randomly tested solutions. Details of the modeling procedure are given by Gallagher (2012). In order to fully exploit the thermal history information contained in partially annealed samples and therefore improve the resolution on the modeling, QTQt is able to model the pre-depositional thermal history of the apatite grains. The final model is represented by a set of time-temperature histories for which we included the expected model (weighted mean model) and the maximum likelihood model (best data fitting model).

5.3. AFT Results

Most samples from the Algeciras/Penibetic/Beni-Ider (CPG4, RON2, RON3, RON7, M5) and Camarote/Nogales/Ubrique units (CPG1, CPG7, and RON5) yielded more than 20 grains, whereas samples from the Aljibe formation, Malaguide (CPG6, RON6, RON8), and CPG3 from the Algeciras formation yielded only a few apatite grains and will not be discussed further (Table 1). In order to assessing population homogeneity, the chi-squared (χ^2) and dispersion tests, with $P(\chi^2)$ values of <0.05 or dispersion values of $>20\%$, are generally used to attest for multiple apatite populations and/or differential annealing kinetics between grains of different composition (e.g., Galbraith & Laslett, 1993). All the eight remaining samples, except RON5, fail the χ^2 test and show moderate to high dispersion and therefore represent mixed ages with different crystals variously affected by annealing.

Radial plots of the distribution of individual grain ages and the grain-age populations shown in Figure 10 are determined by the finite mixture algorithm of Galbraith and Green (1990) implemented in Radialplotter software (Vermeesch, 2009). Except for RON5, the grain-age populations are older than the depositional ages. Systematically, however, a variable but significant proportion of individual grains (30% to 50%) are

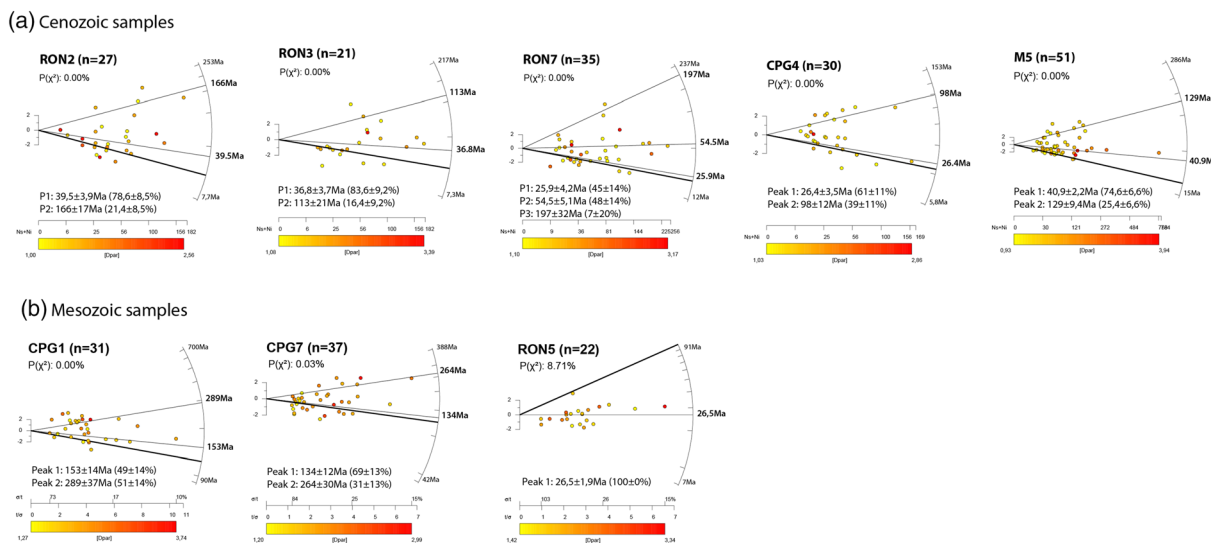


Figure 10. Radial plots of AFT single grain ages (Vermeesch, 2009; 2012) for samples of (a) Lower Miocene and (b) Lower to Middle Cretaceous flysch with more than 20 grains. Yellow to red colors indicate Dpar increasing size. Thick solid line is the stratigraphic age, 22.5 Ma for the Lower Miocene samples, 125 Ma for samples CPG1 and CPG7 and 100 Ma for RON5. Thin solid lines are the single grain-age populations.

younger, within errors, than the depositional ages, indicating our samples recorded post-depositional partial annealing (Figure 10). A component of short track lengths further argues for a period of residence in the partial annealing zone for apatite. No correlation between AFT ages and the Dpar size is observed, which could have indicated an influence of the chemical composition ([Cl]) on the apparent age (Barbarand et al., 2003; Green et al., 1986; O'Sullivan & Parrish, 1995). We infer that the youngest apatite grains are not clearly defined by lower closure temperatures and that source rocks with different thermal evolution could be involved. For RON5, all single grain ages are younger than the late Albian (100 Ma) depositional age with a central age of 26 ± 2 Ma. All other samples are partially annealed (CPG4, RON2, RON3, RON7, M5, CPG1, CPG7) and show two single grain-age populations that are very similar from one sample to the other. For lower Miocene samples (M5, RON2, 3, 7, and CPG4) from the Algeciras Formation, we define an old Cretaceous-to-Jurassic population with age peaks ranging from 98 ± 12 to 166 ± 17 Ma and a younger Paleogene population between 26 ± 3 and 40 ± 3 Ma. Lower Cretaceous samples (CPG1 and CPG7) from Mauretanian series show in addition to Jurassic-Cretaceous populations (153 ± 14 and 134 ± 12 Ma) an older Permian population (264 ± 30 and 289 ± 37 Ma). The consistency of age populations within each set of Miocene and Cretaceous samples suggests they shared a common thermal history and sediment sources.

5.4. Apatite (U-Th-Sm)/He Results

One to nine apatite crystals were selected for each of the 12 samples analysis in order to ensure sample age reproducibility and depending on the apatite quality and the grain dimensions, weight, FT, U, Th, Sm, and He content. Raw and corrected AHe ages are reported in Table 2. AHe analyses performed on Cenozoic samples from the Algeciras formation and Penibetic sandstone (CPG4, CPG3, M5 and RON2, RON3, RON7) yielded between one and 10 grains with ages scattered between 5 and 56 ± 6 Ma. All these samples exhibit several ages younger than, or close to, the stratigraphic age. Samples from the Aljibe formation display similar characteristics but with a much larger spreading of ages, between 15 ± 1 and 210 ± 29 Ma. Cretaceous samples CPG7 and CPG1 yielded nine grains each, spreading from 5 to 99 ± 13 Ma. Single grain ages are always younger than the Cretaceous stratigraphic age (Table 2), indicating substantial post-depositional resetting. RON5 yielded four apatite crystals that are younger than the depositional age. Note that the apatite crystals analyzed here (Table 2) are detrital and therefore originate from different sources as attested by the range of Th/U ratio.

The direct comparison between corrected ages can be more complicated as the damage content that affect the He retentivity (Flowers et al., 2009; Gautheron et al., 2009) can be different even for the same U and

Table 2
Results of (U-Th-Sm)He Analyses on Apatite

Sample	Weight	R_sph	FT	${}^4\text{He}$	U	Th	Sm	eU	Th/U	Age	Corrected age
	(μg)	(μm)		(nccSTP/g)	(ppm)	(ppm)	(ppm)	(ppm)		(Ma)	(Ma)
RON3-A	1.0	34.6	0.6	9.50E+04	18.1	199.3	1045.2	66.0	11.0	11.8	18.9 \pm 2.7
RON3-B	2.5	45.6	0.7	6.83E+04	22.7	122.0	166.5	52.0	5.4	10.9	15.9 \pm 1.9
RON3-C	4.5	58.7	0.8	6.53E+04	5.2	57.3	343.8	19.0	11.0	28.2	35.9 \pm 3.3
RON3-D	4.2	59.8	0.8	9.30E+04	29.7	67.7	546.9	46.0	2.3	16.6	20.8 \pm 1.9
RON7-F	1.5	40.0	0.7	1.09E+04	7.7	32.2	944.4	15.5	4.2	5.5	8.0 \pm 1.0
RON7-G	2.0	42.2	0.7	1.37E+04	22.6	40.4	526.4	32.3	1.8	3.4	5.0 \pm 0.6
RON7-I	2.0	99.7	0.9	1.31E+05	18.0	35.2	267.0	26.4	2.0	40.7	46.7 \pm 3.4
RON7-J	1.1	86.2	0.8	1.97E+05	78.4	283.7	263.3	146.5	3.6	11.2	13.4 \pm 1.1
RON7-L	1.0	34.9	0.7	4.80E+04	23.3	55.9	95.2	36.7	2.4	10.9	16.3 \pm 2.1
RON7-M	1.0	34.7	0.6	7.02E+04	45.4	39.2	224.2	54.8	0.9	10.6	17.4 \pm 2.6
M5-A	1.7	36.8	0.6	3.90E+04	14.7	59.3	106.3	29.0	4.0	11.2	17.7 \pm 2.4
M5-B	2.0	39.2	0.7	4.02E+04	19.1	35.9	213.2	27.9	1.9	12.0	17.7 \pm 2.2
M5-C	5.1	41.0	0.7	5.30E+04	10.9	11.3	95.3	13.7	1.0	32.3	48.4 \pm 6.1
M5-D	3.4	40.9	0.7	2.96E+04	23.5	28.0	128.1	30.3	1.2	8.1	12.2 \pm 1.6
M5-E	3.1	40.6	0.7	2.31E+04	22.7	54.7	123.3	35.9	2.4	5.4	8.1 \pm 1.0
M5-F	1.2	39.5	0.7	2.78E+04	21.9	94.3	218.5	44.6	4.3	5.2	7.9 \pm 1.0
M5-G	1.0	39.0	0.7	3.40E+04	23.4	22.9	320.9	28.9	1.0	9.6	14.7 \pm 1.9
M5-H	1.3	40.5	0.7	3.05E+04	22.7	106.0	226.6	48.2	4.7	5.3	7.6 \pm 0.9
M5-I	1.5	45.0	0.7	4.97E+04	33.9	79.3	297.9	52.9	2.3	7.8	10.7 \pm 1.2
M5-J	2.0	41.6	0.7	8.05E+03	4.3	22.5	189.6	9.7	5.3	6.8	10.0 \pm 1.2
CPG3-D	1.4	32.0	0.6	2.84E+04	22.3	60.9	140.2	37.0	2.7	6.4	10.1 \pm 1.4
CPG4-E	1.5	39.9	0.7	1.77E+05	23.3	60.7	155.6	37.9	2.6	38.6	56.0 \pm 6.7
CPG4-F	1.2	35.5	0.6	1.48E+05	22.0	70.3	1293.8	38.9	3.2	30.4	47.5 \pm 6.4
CPG4-G	2.0	43.5	0.7	4.74E+04	44.2	48.2	961.5	55.8	1.1	6.9	9.6 \pm 1.1
CPG4-H	1.1	33.8	0.6	7.51E+03	7.6	46.5	160.4	18.9	6.1	3.3	5.5 \pm 0.8
CPG4-I	1.3	39.6	0.7	3.05E+05	68.9	180.4	399.6	112.5	2.6	22.6	32.8 \pm 3.9
CPG4-J	1.4	34.1	0.6	2.47E+04	28.1	37.2	97.6	37.1	1.3	5.5	9.2 \pm 1.4
RON8-A	1.6	38.9	0.6	2.57E+05	5.1	41.8	860.8	15.1	8.3	132.7	210.3 \pm 29.2
RON8-B	2.4	45.2	0.7	2.11E+05	16.1	6.6	705.2	17.7	0.4	94.2	133.8 \pm 15.5
RON8-D	8.6	74.0	0.8	1.09E+05	12.6	162.9	483.1	51.7	12.9	17.5	21.4 \pm 1.8
RON8-E	9.5	73.5	0.8	4.15E+04	8.4	20.4	506.5	13.3	2.4	24.9	30.1 \pm 2.5
RON8-F	5.5	61.9	0.8	2.53E+04	9.6	16.8	512.1	13.6	1.8	14.7	19.1 \pm 1.9
RON8-G	4.1	67.1	0.8	2.30E+05	35.9	41.6	469.6	45.9	1.2	41.0	51.8 \pm 4.7
RON8-H	2.6	51.3	0.8	6.35E+04	27.6	74.7	158.0	45.6	2.7	11.6	15.2 \pm 1.5
CPG6-A	4.4	58.0	0.8	2.47E+04	2.1	4.6	10.8	3.2	2.2	63.6	80.3 \pm 7.3
CPG6-B	3.6	52.7	0.7	3.52E+05	30.3	89.0	856.8	51.7	2.9	55.6	76.0 \pm 8.2
RON2-B	2.0	44.1	0.7	4.73E+04	18.2	30.3	1354.8	25.6	1.7	14.5	20.0 \pm 2.2
RON2-C	3.3	51.8	0.7	1.17E+04	3.8	35.9	117.9	12.4	9.5	7.8	10.4 \pm 1.1
RON2-D	4.2	54.8	0.8	1.13E+04	5.1	13.7	586.0	8.4	2.7	10.3	13.5 \pm 1.3
RON5-A	2.0	43.7	0.7	5.11E+04	27.1	65.5	388.6	42.9	2.4	9.8	13.8 \pm 1.6
RON5-B	2.1	43.5	0.7	5.61E+04	19.0	31.6	244.5	26.6	1.7	17.3	24.3 \pm 2.7
RON5-C	2.3	47.8	0.7	3.66E+04	24.8	48.4	886.8	36.5	2.0	8.1	10.9 \pm 1.1
RON5-D	3.2	54.4	0.8	3.15E+04	17.4	39.9	400.8	27.0	2.3	9.5	12.3 \pm 1.2
CPG1-B	7.8	81.4	0.8	1.03E+05	11.4	14.9	178.1	15.0	1.3	56.2	68.6 \pm 5.8
CPG1-C	3.5	52.8	0.8	2.38E+04	6.3	58.1	524.6	20.2	9.3	9.5	12.7 \pm 1.3
CPG1-D	1.8	39.7	0.6	5.54E+04	11.3	69.2	467.4	28.0	6.1	16.2	25.3 \pm 3.4
CPG1-H	2.5	47.3	0.7	5.20E+04	21.1	44.9	807.0	31.8	2.1	13.2	17.8 \pm 1.9
CPG1-J	1.4	41.9	0.7	5.08E+04	9.3	97.8	404.8	32.8	10.5	12.8	18.5 \pm 2.1
CPG1-L	1.0	35.8	0.6	2.11E+05	10.9	71.3	242.5	28.0	6.5	62.1	99.9 \pm 13.8
CPG1-M	1.4	42.9	0.7	4.44E+05	76.7	47.1	459.1	88.0	0.6	41.5	61.0 \pm 7.4
CPG1-N	2.1	58.2	0.8	1.25E+05	36.1	38.9	398.9	45.4	1.1	22.5	30.3 \pm 3.1
CPG1-O	1.7	42.9	0.7	2.04E+04	9.0	68.8	77.2	25.5	7.7	6.7	9.8 \pm 1.2
CPG7-B*	1.7	39.2	0.6	2.66E+04	25.0	152.7	1133.7	61.7	6.1	3.5	5.4 \pm 0.8
CPG7-C	2.1	42.3	0.6	1.20E+04	1.2	53.0	909.3	14.0	44.8	6.7	10.3 \pm 1.4
CPG7-D	2.5	46.8	0.7	4.17E+05	99.1	57.3	753.3	112.9	0.6	30.3	40.8 \pm 4.3
CPG7-E*	2.0	51.2	0.7	1.03E+05	1.8	66.7	513.7	17.9	36.4	46.8	68.5 \pm 8.3
CPG7-F*	2.1	53.0	0.7	9.19E+04	10.1	48.3	1375.9	21.8	4.8	32.7	46.3 \pm 5.3
CPG7-G	0.9	40.4	0.7	7.11E+04	28.3	93.5	349.0	50.8	3.3	11.6	16.3 \pm 1.8
CPG7-H*	1.0	40.4	0.6	2.09E+04	1.2	96.1	466.0	24.2	80.7	7.1	11.2 \pm 1.5

Table 2
Continued

Sample	Weight	R_sph	FT	^4He	U	Th	Sm	eU	Th/U	Age	Corrected age
	(μg)	(μm)		(nccSTP/g)	(ppm)	(ppm)	(ppm)	(ppm)		(Ma)	(Ma)
CPG7-I*	0.8	39.9	0.7	3.16E+04	2.2	71.5	251.2	19.3	33.1	13.5	19.3 ± 2.2
CPG7-J*	0.9	35.2	0.6	1.95E+04	1.8	79.1	119.5	20.8	43.2	7.8	12.1 ± 1.6
RON6-B	0.7	44.2	0.7	1.23E+05	3.8	37.3	26.3	12.7	9.9	80.6	116.8 ± 14.0

Note. Grains marked by an asterisk are grains with relatively high Th/U ratios, these grains were not used for thermal modeling. Underlined grains were not used for thermal modeling based on abnormal ^4He concentrations.

Th content. In fact, the accumulation of damage into each apatite can vary because of different pre-depositional history and chemical composition (Gautheron et al., 2013). Thus, the He-PRZ for each sample can range from 40 to 120°C depending on each crystal (Flowers et al., 2009; Gautheron et al., 2009) and direct comparison with eU content should be taken cautiously. In addition, alpha-implantation from neighbor minerals and undetected rich U-Th inclusions can also increase AHe ages significantly and increase dispersion (e.g., Janowski et al., 2017; Murray et al., 2014; Spiegel et al., 2009). To show the effect of alpha implementation and variety of sources, AHe single grain ages were plotted as a function of the eU content for samples of similar stratigraphic age and formations (Figure 11). In Table 2, AHe data on which doubt exists on the impact of the parameters have been underlined and will not be taken into consideration.

5.5. Modeling of Thermal History

Modeling of the thermal history of AFT data is generally best applied to samples with a single grain-age population. In our case most AFT samples fail the chi-squared test and show two populations that likely reflect multiple sources of apatite (Table 1). Our samples also recorded partial resetting and track lengths reduction during post-depositional heating. To capture the most recent cooling event recorded by the youngest apatite grains and account for the presence of inherited tracks, the models were allowed to explore the pre-depositional thermal histories for all the samples. Additional geological constraints include the stratigraphic ages and assumed depositional palaeotemperatures of the sample, and the present-day temperature of the sample.

Figures 12 and 13 show model results for a selection of AFT-AHe double-dated Cenozoic (RON2, RON3, RON7, M5) and Mesozoic flysch samples (CPG1, CPG7, and RON5) comprising above 20 AFT-dated grains (Figure 10) and measured confined track lengths projected along the *c* axis. To examine how our thermal models reproduce age constraints we also plotted predicted versus observed ages. Models take into account

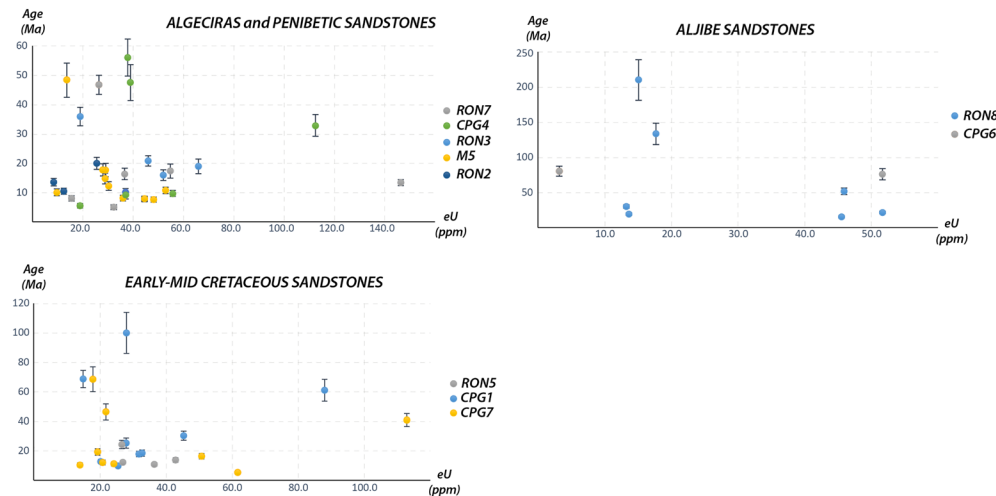


Figure 11. AHe ages plotted against effective uranium (eU) content.

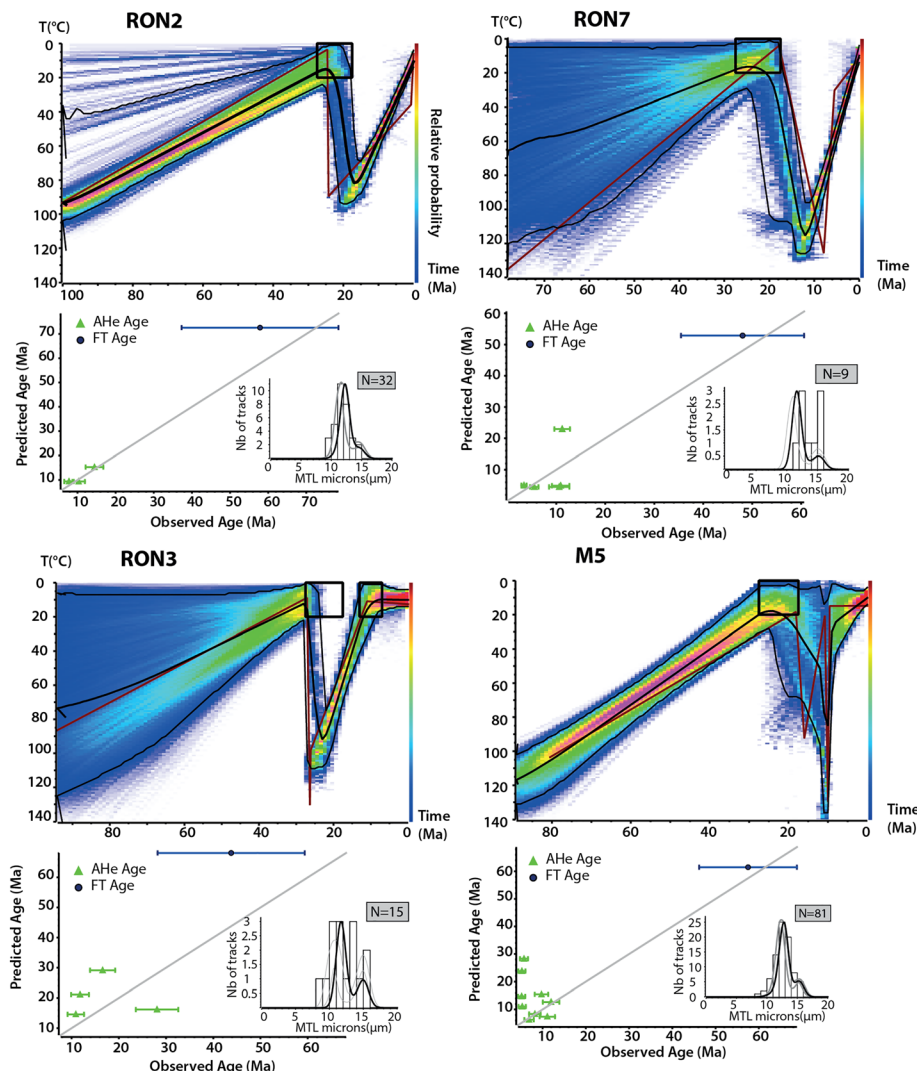


Figure 12. Time-temperature QTQt modeling for Tertiary samples of the Flysch Complex. Colors refer to the probability of a thermal history to pass through a given point. Thin black lines: 95% credible interval; thick black line: expected model; dark red: maximum likelihood model. Associated to each model, relation between predicted and expected AFT and AHe ages and repartition of predicted (thick black line) and measured (histogram) confined Fission Track Length (FTL), N = number of measured confined FTL.

the confined mean track lengths and annealing model of Ketcham et al. (2007) as well as the Dpar value as an indicator of the chlorine content [Cl]. For (U-Th)/He data, each grain is modeled individually incorporating the uncorrected age, grain size, shape, and U, Th, Sm, He concentrations. In most cases, the diffusion model of Flowers et al. (2009), which is better suited for low-damage apatite crystals, yielded models with good resolution.

5.5.1. Thermal History of Cenozoic Flysch Sediments

A wide depositional age of 22.5 ± 5 Ma for the Aljibe, Algeciras and Beni-Ider formations, is assumed to account for all depositional ages published in the literature and conform with stratigraphy shown in Figure 4. All QTQt thermal models show our double-dated samples recorded temperature below 120°C , in agreement with partial resetting (Figure 12) indicated by the proportion of grains younger than depositional age and some short track lengths. They further indicate a short excursion in the partial annealing zone of AFT and fast cooling between 20 and 15 Ma that is reflected by several large track lengths and AHe dates. Only M5 sampled in the Rif domain constrains fast cooling from 10 Ma. RON2, RON7, and M5 reproduce the dispersion of AFT and AHe dates. RON3 from the Penibetic/Subbetic is less well resolved due to the

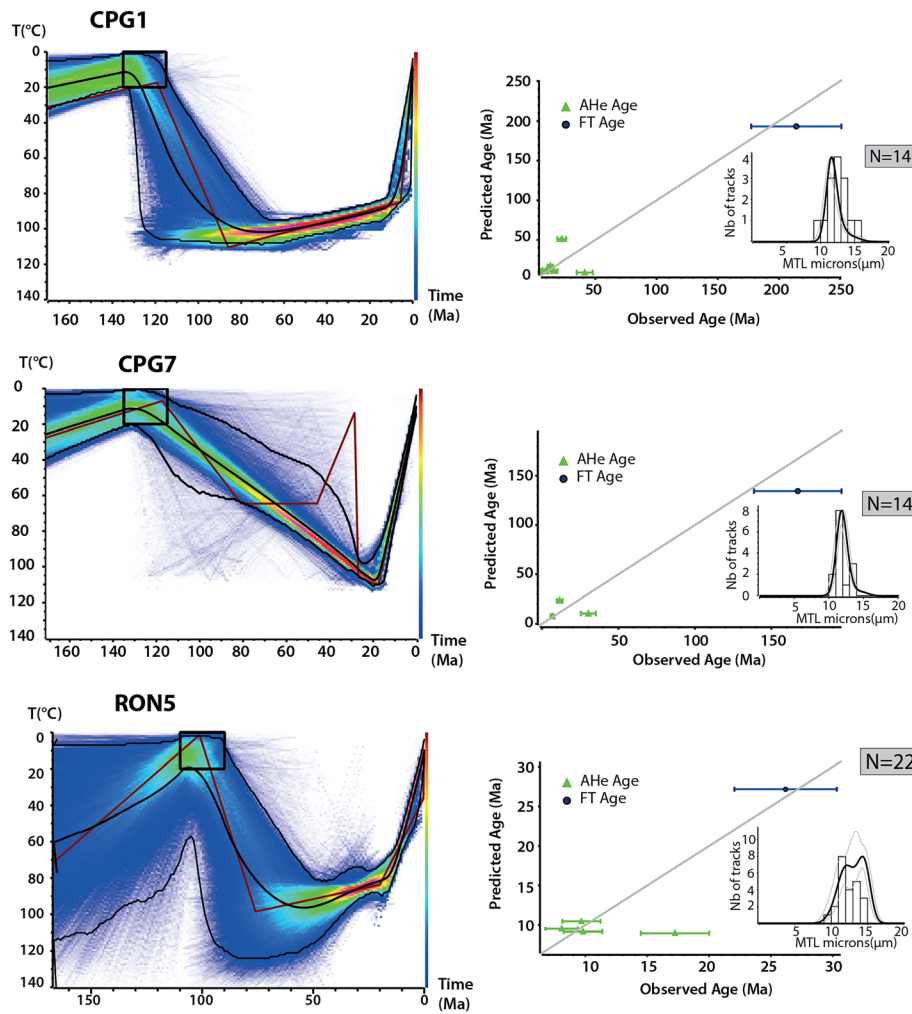


Figure 13. Results of the time temperature QTQt modeling for Tertiary samples of the Flysch Complex.

larger dispersion of AHe dates but the main characteristics of the thermal history are similar to the other Cenozoic flysch deposits. Differences include a slightly earlier exhumation to the surface for RON3 that reflects its stratigraphic position below the upper Miocene (Tortonian-Messinian) marine sediments of the Ronda basin.

5.5.2. Thermal History of Lower Cretaceous Flysch Sediments

Similarly with Cenozoic samples, the partial resetting of Lower Cretaceous samples CPG1, CPG7, and RON5 requires post-depositional heating below 120°C (Figure 12). These samples further resolve thermal histories involving a period of increased cooling from about 15 Ma consistent with Cenozoic samples. The short track lengths of $\sim 10 \mu\text{m}$ indicate apatite grains resided for a prolonged period of time in the partial annealing zone during the upper Cretaceous-Paleogene between 70 and 55 Ma. Both samples CPG1 from the Camarote flysch and RON5 from Ubrique flysch resolve a period of slow cooling in the partial annealing zone of AFT mostly during the Paleogene. CPG7 from Nogales formation shows a distinctive thermal evolution excluding the protracted phase of track lengths reduction during the Paleogene.

In summary, we show that all Cenozoic flysch sediments recorded heating to maximum temperatures of 85 to 120°C, that is in the partial annealing zone for AFT. Two Mesozoic samples show a distinctive time-temperature history indicating sediments underwent a prolonged period of residence between 120 and 60 °C before cooling started most likely during the Paleogene, from 50 Ma. Taking into account the low number of detrital grains dated and the variable duration of residence of sediments in the AFT partial annealing zone suggested by the dispersion of track lengths, we infer all Cenozoic and Mesozoic

samples recorded rapid cooling attributed to rock uplift/exhumation between 20 and 10 Ma in the western Betic and Rif.

6. Discussion

6.1. Early Miocene Cooling in the Flysch Complex: Record of Onset of Post-Orogenic Exhumation

Time-temperature paths obtained from the Mesozoic and Cenozoic flysch series (Figures 12 and 13) give support to a prominent phase of cooling from the uppermost crustal levels in the Burdigalian (20–15 Ma). This timing is consistent regionally with AFT ages of 22–18 Ma from gneiss and schist of the Carratraca massif of the AJ complex (Platt, Argles, et al., 2003) and gneiss and quartzites from ODP well site 976 from the same tectonic unit (Platt & Vissers, 1989). Fission-track analyses performed on the Torrox Unit, from the western AJ complex, confirm rapid cooling between 22 and 18 Ma (350–170°C/Myr) followed by decreasing cooling rates of 5 to 0.5°C/Myr after 17–15 Ma (Andriessen & Zeck, 1996; Zeck et al., 1992). Other fission-track data from the Ojen and Los Reales nappes of the AJ complex north of Marbella (Sierra Blanca and Sierra Alpujata) reveal rapid cooling (>100°C/Myr) in the 19–16 Ma interval (Sosson et al., 1998). This result is further in agreement with detrital AFT ages from Burdigalian-Langhian synorogenic foreland sediments of the Malaguide domain North of the Espuna massif, 500 km to the east of our study area, that record a rapid acceleration of exhumation at about 21 Ma (Lonergan & Johnson, 1998). This is in agreement with the cooling history of AJ complex in the Sierra de Gador (Janowski et al., 2017) also indicating rapid cooling during the late Aquitanian-Burdigalian (23–16 Ma) at rates of 215–245°C/Myr followed by much slower cooling at 16–7.2 Ma at rates of 11–2.5°C/Myr.

Fast exhumation of the Internal Zones is further attested by the late Aquitanian-Burdigalian Ciudad Granada and Viñuela group (Figure 4) containing clasts from the Malaguide and AJ and by the Nava Breccia deposited on the Nieves Unit of the Frontal Units of the Internal Zones (Martín-Algarra, 1987; Serrano et al., 2007). These upper Oligocene-lower Miocene formations are transgressive upon metamorphic complexes of the Alboran domain and therefore reveal nappe stacking of the AJ complex was completed by 22–17 Ma. The Burdigalian cooling detected in the Flysch Complex regionally correlates with extremely rapid cooling event up to 600°C/Myr (e.g., Platt, Argles, et al., 2003) described in the Alboran domain.

Altogether, the Flysch Complex and other sedimentary units from the Internal Zones (Nava Breccia, Ciudad Granada Group, Viñuela Group; see Figure 4) reflect a period of subsidence during the upper Oligocene-lower Miocene followed by rapid uplift/exhumation within a short temporal window between 20 and 15 Ma.

6.2. Pre-Aquitanian Thermal Evolution in the Flysch Complex: A Record of Initial Contraction?

As indicated in section 3 and Figure 3, there is stratigraphic evidence for the onset of foreland flexural subsidence in the Early Eocene (Late Ypresian, ~50 Ma). Ongoing contraction in the external Betic is further consistent with gravitational episodes or erosional unconformities from late Cretaceous up to the early Eocene in the External Zones of the eastern Betic (Guerrera et al., 2006; Martín-Chivelet & Chacón, 2007) and in the Internal Zones by conglomerates sealing upper Eocene thrusts in the Malaguide (Lonergan, 1993). More evidence for this contractional episode are found in the western Betic. In the Corridor de Boyar and Ardite units, Eocene conglomerates were deposited unconformably above the Paleocene (Bourgois, 1978). These sediments reworked Mesozoic material, attesting for an erosional event at this time. Eocene turbidites mapped in the region of Algar and Alcalá de los Gazules further support a marine transgression over the Iberian margin (García de Domingo et al., 1990). Based on these lines of evidence we infer that a period of significant contraction did occur in the Paleogene and likely since the upper Cretaceous.

Thermochronological constraints from the Lower Cretaceous sandstones from the Camarote (CPG1) and from Ubrique (RON5) flysch deposits reveal the upper Cretaceous and sandstones underwent a prolonged period of residence between 120 and 60°C with slow cooling from upper Cretaceous to early Paleogene (70–55 Ma). The weak thermal imprint of this tectonic phase revealed by our apatite low-temperature thermochronology seems inconsistent with a phase of rapid subaerial exhumation. We suggest this initial slow cooling phase occurred in an incipient continental accretionary prism while lower Cretaceous sediments deformed underwater. Such thermal evolution has been documented in pre-orogenic flysch deposits from

other orogens like the Pyrenees and Taiwan (Mesalles et al., 2014; Moutherau et al., 2014; Vacherat et al., 2014) and may also apply here.

Onset of exhumation of HP rocks associated with nappe stacking in the AJ Complex of the eastern Betic (Platt et al., 2005) and in the NF (Augier et al., 2005; Li & Massonne et al., 2018; Monié et al., 1991) is inferred to have started as early as 50 Ma. The temporal concordance between the HP-LT alpine metamorphism, changes in the depositional pattern, and cooling reported from our low-temperature thermochronological data altogether argue for onset of crustal thickening in the latest Cretaceous to early Eocene, leading to the emergence of a proto-Betic domain.

6.3. Allochthony vs. Autochthony of the Flysch Complex With Respect to the Iberian Margin

The migration of the Internal Zones toward the west is classically understood to have led to the deformation of the flysch and formation of the external Betic fold-and-thrust belt in response to trench retreat (Crespo-Blanc & Campos, 2001; Doglioni et al., 1999; Jolivet et al., 2008; Lonergan & White, 1997). In the literature, the Flysch Complex is also typically considered to be allochthonous and being part of the a sedimentary accretionary prism overthrusting the Subbetic, and as such have migrated toward the Guadalquivir basin for several hundred kilometers (Crespo-Blanc & Campos, 2001; Guerrera et al., 1992; Martín-Algarra, 1987; Martín-Algarra et al., 2009). The basal thrust and the important displacement of the Flysch Complex are mostly inferred from stratigraphy and sediments composition that consider the source of flysch deposits as being originated from various places in the Peri-Mediterranean belts (Didon, 1969; Hoyez, 1989; Wildi, 1983). However, our own geological mapping and the work of Flinch and Soto (2017) emphasize that the structure of the Flysch Complex largely reflect salt tectonics rather than large tectonic overthrusting. This leads us to propose an alternative interpretation in which the horizontal displacement experienced by the Flysch Complex is minimized. Cross-sections (e.g., Figure 5) show that the tectonic movements are accommodated by the decoupling in the Triassic allochthonous salt not by the decoupling at the base of the flysch series. Stratigraphy further argued for the existence of a single Eocene to Miocene basin, connecting the Subbetic/Penibetic flysch of the Iberia paleomargin with the deeper facies of the flysch trough. Moreover, our low-temperature data reveal that the Flysch Complex did not reach temperatures higher than 120°C revealing they were buried between 1.3 and 2.6 km (assuming thermal gradient of 30°C/km). The translation of a 2 km-thick flysch nappe over about 800 km, as argued by reconstructions that consider the flysch domain to be originated from a region close to the Balearic Islands, is very unlikely. The preservation of an early Miocene cooling pattern homogeneous in all flysch series (Penibetic RON3 and other Algeciras sandstones RON2, RON7, and M5) indeed do not support such a reconstruction. Together with evidence for Paleogene exhumation and foreland evolution on the Iberian margin, we infer that the Flysch Complex underwent limited displacement. Taking into account the 230 km of N-S shortening expected in the Betic since the upper Cretaceous (Macchiaielli et al., 2017), we infer that a maximum estimate for the displacement of the Flysch Complex should fall in this range.

6.4. A Tectonic Scenario and Geodynamic Implications

Figures 14 and 15 show a spatial and temporal reconstruction of the geodynamic evolution of the Betic-Rif region from early Cretaceous rifting stage to late Tortonian contraction.

Rifting during late Triassic to early Jurassic between central Atlantic and Alpine Tethys and during late Jurassic to early Cretaceous times (Angrand et al., 2020; Dercourt et al., 1986; Handy et al., 2010; Labails et al., 2010; Leprêtre et al., 2018; Martín-Algarra, 1987) led to the formation of several basins between Africa and Iberia. They correspond to the Subbetic (e.g., Crespo-Blanc & de Lamotte, 2006; Jabaloy-Sánchez et al., 2019), the Algarve basin (e.g., Ramos et al., 2016), the Cretaceous flysch basin, stretching along the transform plate boundary between Africa and Iberia, and the external Rif and Ketama basins (Durand-Delga, 1972; Wildi, 1983). Extension resulted in mantle exhumation in the external Rif, in the former Cretaceous Flysch basin, in the Gorringe Bank and in the NF (Durand-Delga et al., 2000; Jiménez-Munt et al., 2011; Michard et al., 1992; Puga et al., 2002). In our reconstruction, the Cretaceous flysch basin corresponds to the most distal part of the Iberian margin. It is laterally connected to the flysch series of the Ketama basin (Figures 14 and 15).

Following the onset of convergence between Eurasia and Africa at 84 Ma, contractional deformation is recorded in the Malaguide by a transgression and onset of flexural subsidence at about 50 Ma (e.g.,

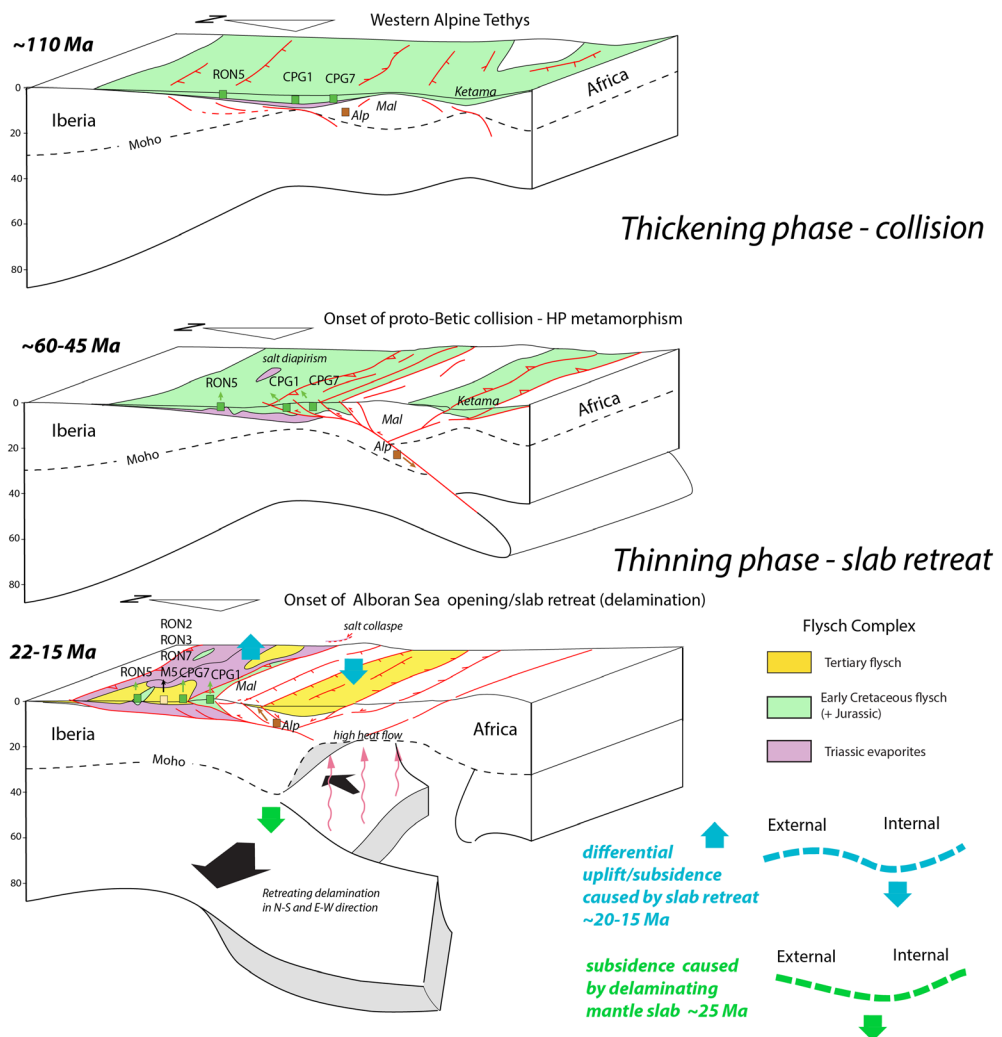


Figure 14. Geodynamic reconstructions depicting the evolution of the western Betic domain, with a focus on the Flysch Complex, salt tectonics, and location of thermochronological samples (green, yellow, and brown squares).

Figure 3, Hanne et al., 2003; Maaté et al., 2000), in North-Africa (Frizon de Lamotte et al., 2000, 2011; Leprêtre et al., 2018) (Figures 14, 15; 60–45 Ma) and in the Guadalquivir and Gorringe Bank (Ramos et al., 2017).

Onset of foreland subsidence in the early Eocene is outlined by transgression and deposition of nummulitic limestones preserved in the Malaguide (Figures 14, 15; 60–45 Ma). This stage is followed by the deposition of deep-marine sediments during the middle to late Eocene throughout the Betics (Lonergan & Mange-Rajetzky, 1994, and Figure 4). Crustal thickening required to produce flexural subsidence in the Malaguide is coeval with cooling recorded in the Mesozoic flysch (samples CPG1 and RON5) and onset of S-vergent underthrusting of the Iberia crust suggested by several Paleogene ages for peak HP metamorphism (see section 2).

The contraction of the Iberia paleomargin at this time is consistent with the far-field deformation recorded from the Atlas (e.g., Leprêtre et al., 2018), exhumation in the Anti-Atlas (Sehrt et al., 2018), and evidence for contraction throughout Iberia, including the Iberian Range (Rat et al., 2019) and the Pyrenees (e.g., Mouthereau et al., 2014). In order to be consistent with estimates of N-S directed Africa-Iberia convergence (Machiavelli et al., 2017) in southern Iberia, the Internal Zones of the proto-AlKaPeCa/Mesomediterranean domain have been restored by 200–250 km in the east/south-east direction (Figures 14, 15; 60–45 Ma). This amount is accommodated by up to 150 km of NW/SE-directed contraction in the western Betics of which we

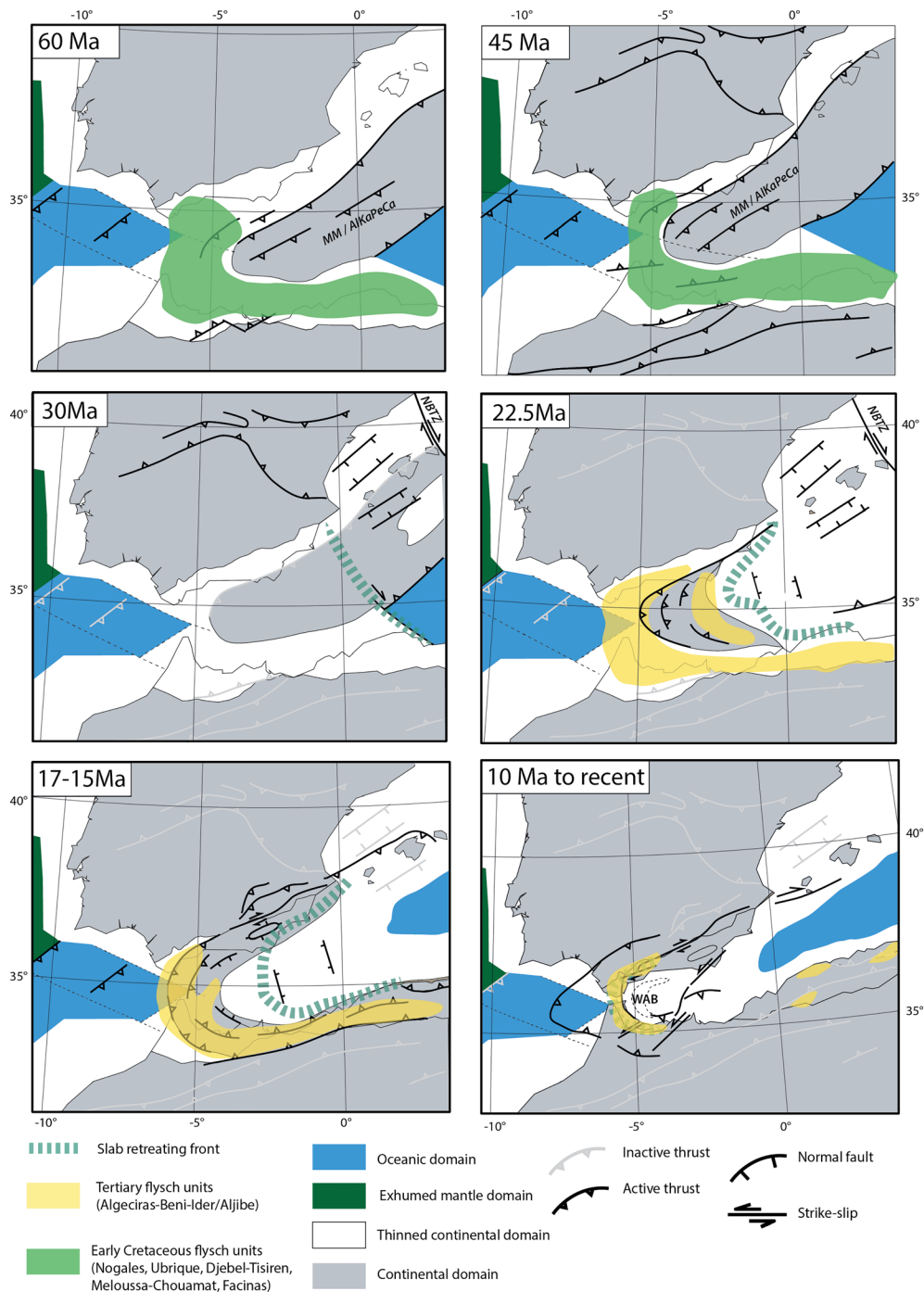


Figure 15. Paleogeography of the flysch series in the geodynamic evolution of the Betic-Rif region since 60 Ma. Thick red dashed line shows the approximate location of the cross sections of Figure 15. This reconstruction was drawn using the kinematic reconstruction of Müller et al. (2016). Large-scale deformations in Iberia and Africa are redrawn after Leprêtre et al. (2018). Continental, transitional, or oceanic domains are from Ramos et al. (2017) and Nirrengarten et al. (2018). MM/proto-AlKaPeCa = Mesomediterranean domain-AlKaPeCa domain.

must add 100 km of EW-directed extension inferred from restoration of low-angle detachment system in Sierra Nevada and Sierra de los Filabres metamorphic domes (Martínez-Martínez et al., 2002).

Our reconstruction is consistent with Vergés and Fernandez (2012), placing the south-vergent subduction to the south of the paleomargin of Iberia in upper Cretaceous to Paleogene. However, stratigraphy, structure,

and thermochronological constraints suggest to place proto-AlKaPeCa domain closer to Iberia. Because 200–250 km of shortening is accommodated in the Betics, our reconstruction implies that the 600 km-long slab imaged beneath the arc (Bezada et al., 2013; Fichtner & Villaseñor, 2015; Mancilla et al., 2015; Palomeras et al., 2017; Spakman & Wortel, 2004; Villaseñor et al., 2015) corresponds to a delaminated mantle slab. Mantle delamination model is similar to the retreating delamination models by Calvert et al. (2000) and Petit et al. (2015), and was also suggested by Roure et al. (2012) for the North African margin.

The Oligocene stage (30 Ma) marks a transitional period during which the tectonic regime changed from contractional to extensional in the Western Mediterranean (Jolivet et al., 2008; Figures 14 and 15). Subsidence analyses (Figure 3) suggest that flexural subsidence driven by increasing tectonic load and/or slab pull persisted at least until the late Oligocene. The roll-back of the Tethys Ocean in the East is thought to have started in a subduction zone positioned south of the Balearic Islands (e.g., Jolivet et al., 2008). Slab retreat in the east then triggered backarc extension to the west in the proto-Alboran domain. Lithospheric transfer zones required to accommodate the differential extension between the Mediterranean region and proto-Alboran domain may have triggered delamination at the origin of the Alboran sea.

The onset of the west-directed retreating mantle delamination most likely initiated in the Burdigalian at the latest as constrained by the timing of extension and westward migration of the Alboran domain (see section 3).

Around 22.5 Ma, there is a general subsidence associated with the deposition (and heating) of the flysch series of Algeciras and Aljibe formations and in the Penibetic/subbetic coevally with the deposition of the Ciudad Granada group on top of the internal Alboran domains. We propose that this downward regional movement of the external and internal domains reflect the pulling forces arising from the sinking delaminated mantle (Figures 14 and 15). Such a large subsidence of both the flysch series above the internal domains can still be observed in the WAB where the mantle slab is still attached and pulls the crust down (Couto et al., 2016; see also Figure 2). As delamination migrated, compressional deformation propagated toward the external domains, resulting in exhumation of the previously subsident flysch basin as indicated by regional cooling event at 20–15 Ma. The innermost Alboran domain underwent a coeval thinning and heating caused by the asthenospheric upwelling (Figure 14), followed by fast thermal reequilibration and denudation of Internal Zones responsible for the clustering of geochronological ages around 22–19 Ma.

Exhumation caused remobilization and collapse of the flysch series above the thick Triassic gypsum at the origin of tectono-sedimentary mélanges. After late Burdigalian, subsidence resumed in the early Tortonian (Figure 15; 17–15 Ma) as recorded by marine sedimentation in the Ronda extensional basin. Tortonian was associated with orogen-parallel extension that also affected a large portion of the Flysch Complex and External Zones through normal faulting and strike-slip movements (e.g., Crespo-Blanc et al., 2016; Jimenez-Bonilla et al., 2016). This late extension was followed by a NNW-SSE-directed compression associated with the tightening of the arc from the late Tortonian onward (Figure 15; 10 Ma) and westward expulsion of the Alboran domain (e.g., Crespo-Blanc et al., 2016). From the late Messinian (5.3 Ma) onward, transition from marine to continental sedimentation occurred in the Ronda basin and in all the Internal Zones of the Betics. This event was associated with general uplift of up to 1,000 m of the intramontane Neogene basins (Iribarren et al., 2009; Janowski et al., 2017) triggered by westward propagation of slab tearing (or detachment) below the Betics (Mancilla et al., 2015; Spakman & Wortel, 2004).

7. Conclusions

The aim of this paper was to better understand the poorly constrained, earliest stage of deformation in the Betics, and to discuss the temporal and spatial evolution of the Flysch Complex, a key element to understand the Betic-Rif geodynamics. Based on the existing stratigraphic constraints, evidence for the imprint of salt tectonics on the structure of the Flysch Complex, and new low-temperature thermochronological data, we argue that a Paleogene stage of deformation affected both the Iberian paleomargin and the Internal Zones. Time-temperature histories from Cretaceous flysch (Ubrique-Boyar Flysch) deposited on the distal Iberian paleomargin show cooling occurred at ca. 50 Ma. These new constraints support a pre-Oligocene phase of orogenic growth in the Betic Cordillera in accord with the acceleration of the subsidence in the foreland. The exhumation of the Flysch Complex occurred between 20 and 15 Ma coherent with rapid exhumation of the internal metamorphic complexes. This finding further supports a geodynamic reconstruction in

which the Flysch Complex and Internal Zones formed in a proto-Betic orogenic domain positioned close to the present-day Alboran domain. To account for the synchronous early Miocene cooling of the Flysch Complex and the Internal Zones we suggest that extension in the Alboran domain was driven by the westward drift of a delaminated mantle slab from beneath a proto-Betic orogenic segment.

Acknowledgments

We gratefully acknowledge discussion and support from the Centre National de la Recherche Scientifique (CNRS), the French Geological Survey (BRGM), and TOTAL through the OROGEN project. Comments by William Cavazza on an earlier version greatly improved the quality of the manuscript. The detailed review by Martín-Algarra provided very useful insights on the stratigraphy of the western Betic Cordillera and additional comments by anonymous reviewers led to improve the final version of the manuscript. We also thank Jose Miguel Azafón, Guillermo Booth-Rea from the University of Granada, and Najib Zaghoul from Abdelmalek Essaâdi University and his PhD student, Anas Abbassi for their support in the field, scientific discussions, and warm welcome during our stay in Morocco. Thanks also to Dominique Frizon de Lamotte who made the field trip in Morocco possible. Rosella Pinna Jamme and Frédéric Haurine (GEOPS) are thanked for their help for the (U-Th-Sm)/He and ICPMS analyses. All data presented in this article are shared and made freely available on the open-access repository Zenodo (doi 10.5281/zenodo.3872083).

References

- Alcalá-García, F. J., López-Galindo, A., & Martín-Martín, M. (2002). El paleoceno de la alta cadena (subbetico interno, Cordillera Bética) implicaciones en la evolución geodinámica del paleomargen sud-iberico. *Estudios Geológicos*, 58(3–4), 75–85. <https://doi.org/10.3989/egeol.02583-4112>
- Andriessen, P. A. M., & Zeck, H. P. (1996). Fission-track constraints on timing of Alpine nappe emplacement and rates of cooling and exhumation, Torrox area, Betic Cordilleras, S. Spain. *Chemical Geology*, 131(1–4), 199–206. [https://doi.org/10.1016/0009-2541\(95\)00148-4](https://doi.org/10.1016/0009-2541(95)00148-4)
- Angrand, P., Mouthereau, F., Masini, E., & Asti, R. (2020). A reconstruction of Iberia accounting for W-Tethys/N-Atlantic kinematics since the late Permian-Triassic. *Solid Earth Discussions*. <https://doi.org/10.5194/se-2020-24>
- Augier, R., Agard, P., Monié, P., Jolivet, L., Robin, C., & Booth-Rea, G. (2005). Exhumation, doming and slab retreat in the Betic Cordillera (SE Spain): In situ 40Ar/39Ar ages and P-T-d-t paths for the Nevado-Filabride complex. *Journal of Metamorphic Geology*, 23(5), 357–381. <https://doi.org/10.1111/j.1525-1314.2005.00581.x>
- Barbarand, J., Carter, A., Wood, I., & Hurford, T. (2003). Compositional and structural control of fission-track annealing in apatite. *Chemical Geology*, 198(1–2), 107–137. [https://doi.org/10.1016/S0009-2541\(02\)00424-2](https://doi.org/10.1016/S0009-2541(02)00424-2)
- Berástegui, X., Banks, C. J., Puig, C., Taberner, C., Waltham, D., & Fernández, M. (1998). Lateral diapiric emplacement of Triassic evaporites at the southern margin of the Guadalquivir Basin, Spain. *Geological Society, London, Special Publications*, 134(1), 49–68. <https://doi.org/10.1144/GSL.SP.1998.134.01.04>
- Bezada, M. J., Humphreys, E. D., Toomey, D. R., Harnafi, M., Dávila, J. M., & Gallart, J. (2013). Evidence for slab rollback in westernmost Mediterranean from improved upper mantle imaging. *Earth and Planetary Science Letters*, 368, 51–60. <https://doi.org/10.1016/j.epsl.2013.02.024>
- Booth-Rea, G., Azafón, J. M., Goffé, B., Vidal, O., & Martínez-Martínez, J. M. (2002). High-pressure, low-temperature metamorphism in Alpujarride units of southeastern Betics (Spain). *Comptes Rendus Geoscience*, 334(11), 857–865. [https://doi.org/10.1016/S1631-0713\(02\)01787-X](https://doi.org/10.1016/S1631-0713(02)01787-X)
- Bourgois, J. (1978). *Etude géologique de la transversale de Ronda (Cordillères bétiques, Espagne), données géologiques pour un modèle d'évolution de l'arc de Gibraltar*. Thèse d'Etat, Géologie structurale. Université de Besançon.
- Bourgois, J., & Chauve, P. (1971). Le Corridor de Boyar et ses abords, leur place dans l'Ouest des Cordillères bétiques. *Revue de Géographie Physique et de Géologie Dynamique*, 2(13), 463–488.
- Calvert, A., Sandvol, E., Seber, D., Barazangi, M., Roecker, S., Mourabit, T., et al. (2000). Geodynamic evolution of the lithosphere and upper mantle beneath the Alboran region of the western Mediterranean: Constraints from travel time tomography. *Journal of Geophysical Research*, 105(B5), 10,871–10,898. <https://doi.org/10.1029/2000JB900024>
- Chalouan, A., El Mrihi, A., El Kadiri, K., Bahmad, A., Salhi, F., & Hilal, R. (2006). Mauretanian flysch nappe in the northwestern Rif Cordillera (Morocco): Deformation chronology and evidence for a complex nappe emplacement. *Geological Society, London, Special Publications*, 262(1), 161–175. <https://doi.org/10.1144/GSL.SP.2006.262.01.10>
- Comas, M. C., Platt, J. P., Soto, J. I., & Watts, A. B. (1999). The origin and tectonic history of the Alboran Basin: Insights from Leg 161 results. In R. Zahn, M. C. Comas, & A. Klaus (Eds.), *Proc. ODP, Sci. Results*, 161 (pp. 555–580). College Station, TX: Ocean Drilling Program. <https://doi.org/10.2973/odp.proc.sr.161.262.1999>
- Couto, D., Gorini, C., Jolivet, L., Lebret, N., Augier, R., Gumiaux, C., et al. (2016). Tectonic and stratigraphic evolution of the Western Alboran Sea Basin in the last 25 Myrs. *Tectonophysics*, 677–678, 280–311. <https://doi.org/10.1016/j.tecto.2016.03.020>
- Crespo-Blanc, A., & Campos, J. (2001). Structure and kinematics of the South Iberian paleomargin and its relationship with the Flysch Trough units: Extensional tectonics within the Gibraltar Arc fold-and-thrust belt (western Betics). *Journal of Structural Geology*, 23(10), 1615–1630. [https://doi.org/10.1016/S0191-8141\(01\)00012-8](https://doi.org/10.1016/S0191-8141(01)00012-8)
- Crespo-Blanc, A., Comas, M., & Balanyá, J. C. (2016). Clues for a Tortonian reconstruction of the Gibraltar Arc: Structural pattern, deformation diachronism and block rotations. *Tectonophysics*, 683, 308–324. <https://doi.org/10.1016/j.tecto.2016.05.045>
- Crespo-Blanc, A., & de Lamotte, D. F. (2006). Structural evolution of the external zones derived from the Flysch trough and the South Iberian and Maghrebian paleomargins around the Gibraltar Arc: A comparative study. *Bulletin de la Société géologique de France*, 177(5), 267–282. <https://doi.org/10.2113/gssgbull.177.5.267>
- Dercourt, J. E. A., Zonenshain, L. P., Ricou, L. E., Kazmin, V. G., Le Pichon, X., Knipper, A. L., et al. (1986). Geological evolution of the Tethys belt from the Atlantic to the Pamirs since the Liás. *Tectonophysics*, 123(1–4), 241–315. [https://doi.org/10.1016/0040-1951\(86\)90199-X](https://doi.org/10.1016/0040-1951(86)90199-X)
- Didon, J. (1969). *Etude géologique du Campo de Gibraltar*. Thèse (p. 539). Univ. Paris.
- Didon, J., Durand-Delga, M., & Kornprobst, J. (1973). Homologies géologiques entre les deux rives du détroit de Gibraltar. *Bulletin de la Société géologique de France*, S7-XV(2), 77–105. <https://doi.org/10.2113/gssgbull.s7-xv.2.77>
- Doglioni, C., Fernandez, M., Gueguen, E., & Sabat, F. (1999). On the interference between the early Apennines-Maghrebides backarc extension and the Alps-Betics orogen in the Neogene Geodynamics of the Western Mediterranean. *BOLLETTINO-SOCIETÀ GEOLOGICA ITALIANA*, 118, 75–90.
- Durand Delga, M., & Foucault, A. (1967). La Dorsale bétique, nouvel élément paléogéographique et structural des Cordillères bétiques, au bord sud de la Sierra Arana (prov. de Grenade, Espagne). *Bulletin de la Société Géologique de France*, S7-IX(5), 723–728. <https://doi.org/10.2113/gssgbull.s7-ix.5.723>
- Durand-Delga, M. (1972). La courbure de Gibraltar, extrémité occidentale des chaînes alpines, unit l'Europe et l'Afrique. *Eclogae Geologicae Helvetiae*, 65(2), 267–278.
- Durand-Delga, M., Rossi, P., Olivier, P., & Puglisi, D. (2000). Situation structurale et nature ophiolitique de roches basiques jurassiques associées aux flyschs maghrébins du Rif (Maroc) et de Sicile (Italie). *Comptes Rendus de l'Académie des Sciences - Series IIa - Earth and Planetary Science*, 331(1), 29–38. [https://doi.org/10.1016/s1251-8050\(00\)01378-1](https://doi.org/10.1016/s1251-8050(00)01378-1)

- Esteban, J. J., Cuevas, J., Tubía, J. M., Gutiérrez-Alonso, G., Larionov, A., Sergeev, S., & Hofmann, M. (2017). U-Pb detrital zircon ages from the Paleozoic Marbella Conglomerate of the Malaguide Complex (Betic Cordilleras, Spain) Implications on Paleotethyan evolution. *Lithos*, 290, 34–47. <https://doi.org/10.1016/j.lithos.2017.07.022>
- Esteban, J. J., Sánchez-Rodríguez, L., Seward, D., Cuevas, J., & Tubía, J. M. (2004). The late thermal history of the Ronda area, southern Spain. *Tectonophysics*, 389(1–2), 81–92. <https://doi.org/10.1016/j.tecto.2004.07.050>
- Ehlers, T., & Farley, K. (2003). Apatite (U-Th)/He thermochronometry: Methods and applications to problems in tectonic and surface processes. *Earth and Planetary Science Letters*, 206(1–2), 1–14. [https://doi.org/10.1016/s0012-821x\(02\)01069-5](https://doi.org/10.1016/s0012-821x(02)01069-5)
- Faccenna, C., Becker, T. W., Luente, F. P., Jolivet, L., & Rossetti, F. (2001). History of subduction and back arc extension in the Central Mediterranean. *Geophysical Journal International*, 145(3), 809–820. <https://doi.org/10.1046/j.0956-540x.2001.01435.x>
- Feinberg, H., & Olivier, P. (1983). Datation de termes aquitanians et burdigaliens dans la zone prédorsaliennes bético-rifaine et ses conséquences. *Comptes Rendus de l'Académie des Sciences, Série IIa, Sciences de la Terre et des Planètes*, 296, 473–476.
- Fichtner, A., & Villaseñor, A. (2015). Crust and upper mantle of the western Mediterranean—Constraints from full-waveform inversion. *Earth and Planetary Science Letters*, 428, 52–62. <https://doi.org/10.1016/j.epsl.2015.07.038>
- Fillon, C., Gautheron, C., & Beek, P. (2013). Oligocene–Miocene burial and exhumation of the Southern Pyrenean foreland quantified by low-temperature thermochronology. *Journal of the Geological Society*, 170(1), 67–77. <https://doi.org/10.1144/jgs2012-051>
- Flinch, J. F., Bally, A. W., & Wu, S. (1996). Emplacement of a passive-margin evaporitic allochthon in the Betic Cordillera of Spain. *Geology*, 24(1), 67–70. [https://doi.org/10.1130/0091-7613\(1996\)024<0067:EOAPME>2.3.CO;2](https://doi.org/10.1130/0091-7613(1996)024<0067:EOAPME>2.3.CO;2)
- Flinch, J. F., & Soto, J. I. (2017). Chapter 19 - Allochthonous Triassic and Salt Tectonic Processes in the Betic-Rif Orogenic Arc. In J. I. Soto, J. F. Flinch, & G. Tari (Eds.), *Permo-Triassic Salt Provinces of Europe, North Africa and the Atlantic Margins* (pp. 417–446). <https://doi.org/10.1016/B978-0-12-809417-4.00020-3>
- Flowers, R. M., Ketcham, R. A., Shuster, D. L., & Farley, K. A. (2009). Apatite (U-Th)/He thermochronometry using a radiation damage accumulation and annealing model. *Geochimica et Cosmochimica Acta*, 73(8), 2347–2365. <https://doi.org/10.1016/j.gca.2009.01.015>
- Frasca, G., Gueydan, F., & Brun, J. P. (2015). Structural record of Lower Miocene westward motion of the Alboran Domain in the Western Betics, Spain. *Tectonophysics*, 657, 1–20. <https://doi.org/10.1016/j.tecto.2015.05.017>
- Frizon de Lamotte, D., Raulin, C., Mouchot, N., Wrobel-Daveau, J. C., Blanpied, C., & Ringenbach, J. C. (2011). The southernmost margin of the Tethys realm during the Mesozoic and Cenozoic: Initial geometry and timing of the inversion processes. *Tectonics*, 30, TC3002. <https://doi.org/10.1029/2010TC002691>
- Frizon de Lamotte, D., Saint Bezat, B., Bracène, R., & Mercier, E. (2000). The two main steps of the Atlas building and geodynamics of the western Mediterranean. *Tectonics*, 19(4), 740–761. <https://doi.org/10.1029/2000TC900003>
- Galbraith, R. F., & Green, P. F. (1990). Estimating the component ages in a finite mixture. *International Journal of Radiation Applications and Instrumentation Part D. Nuclear Tracks and Radiation Measurements*, 17(3), 197–206. [https://doi.org/10.1016/1359-0189\(90\)90035-V](https://doi.org/10.1016/1359-0189(90)90035-V)
- Galbraith, R. F., & Laslett, G. M. (1993). Statistical models for mixed fission track ages. *Nuclear Tracks and Radiation Measurements*, 21(4), 459–470. [https://doi.org/10.1016/1359-0189\(93\)90185-C](https://doi.org/10.1016/1359-0189(93)90185-C)
- Gallagher, K. (2012). Transdimensional inverse thermal history modeling for quantitative thermochronology. *Journal of Geophysical Research*, 117, B02408. <https://doi.org/10.1029/2011JB008825>
- García de Domingo, González, L. J., Hernaiz, H. P. P., Zazo, C., & Goy, G. J. L. (1990). *Mapa Geológico de España 1: 50.000, hoja nº 1073 (Vejor de la Frontera)*. Instituto Geológico y Minero de España.
- García-Hernández, M., López-Garrido, A., Rivas, P., Galdeano, C., & Vera, J. (1980). Mesozoic palaeogeographic evolution of the External Zones of the Betic Cordillera. *Geologie en Mijnbouw*, 59(2), 155–168.
- Gautheron, C., Barbarand, J., Ketcham, R., Tassan-Got, L., Beek, P., Pagel, M., et al. (2013). Chemical influence on α -recoil damage annealing in apatite: Implications for (U-Th)/He dating. *Chemical Geology*, 351, 257–267. <https://doi.org/10.1016/j.chemgeo.2013.05.027>
- Gautheron, C., & Tassan-Got, L. (2010). A Monte Carlo approach to diffusion applied to noble gas/helium thermochronology. *Chemical Geology*, 273(3–4), 212–224. <https://doi.org/10.1016/j.chemgeo.2010.02.023>
- Gautheron, C., Tassan-Got, L., Barbarand, J., & Pagel, M. (2009). Effect of alpha-damage annealing on apatite (U-Th)/He thermochronology. *Chemical Geology*, 266(3–4), 157–170. <https://doi.org/10.1016/j.chemgeo.2009.06.001>
- Goffe, B., Michard, A., García-Duñas, V., Gonzalez-Lodeiro, F., Monie, P., Campos, J., et al. (1989). First evidence of high-pressure, low-temperature metamorphism in the Alpujárride nappes, Betic Cordilleras (S.E. Spain). *European Journal of Mineralogy*, 1(1), 139–142. <https://doi.org/10.1127/ejm/01/01013>
- Gómez-Pugnaire, M. T., & Fernández-Soler, J. M. (1987). High-pressure metamorphism in metabasites from the Betic Cordilleras (SE Spain) and its evolution during the Alpine orogeny. *Contributions to Mineralogy and Petrology*, 95(2), 231–244. <https://doi.org/10.1007/BF00381273>
- Gómez-Pugnaire, M. T., Rubatto, D., Fernández-Soler, J. M., Jabaloy, A., López-Sánchez-Vizcaíno, V., González-Lodeiro, F., et al. (2012). Late Variscan magmatism in the Nevado-Filábride Complex: U-Pb geochronologic evidence for the pre-Mesozoic nature of the deepest Betic complex (SE Spain). *Lithos*, 146, 93–111. <https://doi.org/10.1016/j.lithos.2012.03.027>
- Green, P. F., Duddy, I. R., Gleadow, A. J. W., Tingate, P. R., & Laslett, G. M. (1986). Thermal annealing of fission tracks in apatite: 1 A qualitative description. *Chemical Geology: Isotope Geoscience*, 59, 237–253. [https://doi.org/10.1016/0168-9622\(86\)90074-6](https://doi.org/10.1016/0168-9622(86)90074-6)
- Guerrera, F., Estévez, A., López-Arcos, M., Martín-Martín, M., Martín-Pérez, J. A., & Serrano, F. (2006). Paleogene tectono-sedimentary evolution of the Alicante Trough (External Betic Zone, SE Spain) and its bearing on the timing of the deformation of the South-Iberian Margin. *Geodinamica Acta*, 19(2), 87–101. <https://doi.org/10.3166/ga.19.87-101>
- Guerrera, F., Loiacono, F., Puglisi, D., & Moretti, E. (1992). The Numidian nappe in the Maghrebian Chain: State of the art. *Bollettino della Società Geologica Italiana*, 111(2), 217–253.
- Guerrera, F., & Martín-Martín, M. (2014). Geodynamic events reconstructed in the Betic, Maghrebian, and Apennine chains (central-western Tethys). *Bulletin de la Société Géologique de France*, 185(5), 329–341. <https://doi.org/10.2113/gssgbull.185.5.329>
- Handy, M. R., Schmid, S. M., Bousquet, R., Kissling, E., & Bernoulli, D. (2010). Reconciling plate-tectonic reconstructions of Alpine Tethys with the geological-geophysical record of spreading and subduction in the Alps. *Earth-Science Reviews*, 102(3–4), 121–158. <https://doi.org/10.1016/j.earscirev.2010.06.002>
- Hanne, D., White, N., & Lonergan, L. (2003). Subsidence analyses from the Betic Cordillera, southeast Spain. *Basin Research*, 15(1), 1–21. <https://doi.org/10.1046/j.1365-2117.2003.00192.x>
- Hoyez, B. (1989). *Le Numidien et les flyschs oligo-miocènes de la bordure sud de la Méditerranée occidentale*. Thèse (pp. 1–459). Lille: Univ. de Lille.

- Hurford, A. J., & Green, P. F. (1983). The zeta age calibration of fission-track dating. *Chemical Geology*, 41, 285–317. [https://doi.org/10.1016/S0009-2541\(83\)80026-6](https://doi.org/10.1016/S0009-2541(83)80026-6)
- Iribarren, L., Vergés, J., & Fernandez, M. (2009). Sediment supply from the Betic–Rif orogen to basins through Neogene. *Tectonophysics*, 475(1), 68–84. <https://doi.org/10.1016/j.tecto.2008.11.029>
- Jabaloy-Sánchez, A., Martín-Algarra, A., Padrón-Navarta, J., Martín-Martín, M., Gómez-Pugnaire, M., Sánchez-Vizcaíno, V., & Garrido, C. (2019). Lithological successions of the Internal Zones and Flysch Trough units of the Betic Chain. In C. Quesada, & J. Oliveira (Eds.), *The Geology of Iberia: A Geodynamic Approach* (Chap. 8, pp. 377–432). Cham: Regional Geology Reviews, Springer.
- Jackson, M. P., & Hudec, M. R. (2017). *Salt tectonics: Principles and practice*. Cambridge: Cambridge University Press.
- Janowski, M., Loget, N., Gautheron, C., Barbarand, J., Bellahsen, N., Van den Driessche, J., et al. (2017). Neogene exhumation and relief evolution in the eastern Betics (SE Spain): Insights from the Sierra de Gador. *Terra Nova*, 29(2), 91–97. <https://doi.org/10.1111/ter.12252>
- Jimenez-Bonilla, A., Torvela, T., Balanyá, J., Expósito, I., & Díaz-Azpiroz, M. (2016). Changes in dip and frictional properties of the basal detachment controlling orogenic wedge propagation and frontal collapse: The external central Betics case: Basal Dip and Frictional Properties. *Tectonics*, 35, 3028–3049. <https://doi.org/10.1002/2016tc004196>
- Jiménez-Munt, I., Fernández, M., Vergés, J., García-Castellanos, D., Fullea, J., Pérez-Gussinyé, M., & Afonso, J. (2011). Decoupled crust–mantle accommodation of Africa-Eurasia convergence in the NW Moroccan margin. *Journal of Geophysical Research*, 116. <https://doi.org/10.1029/2010jb008105>
- Johnson, C. (1997). Resolving denudational histories in orogenic belts with apatite fission-track thermochronology and structural data: An example from southern Spain. *Geology*, 25(7), 623–626. [https://doi.org/10.1130/0091-7613\(1997\)025<0623:RDHIOB>2.3.CO;2](https://doi.org/10.1130/0091-7613(1997)025<0623:RDHIOB>2.3.CO;2)
- Jolivet, L., Augier, R., Faccenna, C., Negro, F., Rimmele, G., Agard, P., et al. (2008). Subduction, convergence and the mode of backarc extension in the Mediterranean region. *Bulletin de la Société Géologique de France*, 179(6), 525–550. <https://doi.org/10.2113/gssgbull.179.6.525>
- Ketcham, R. A., Carter, A., Donelick, R. A., Barbarand, J., & Hurford, A. J. (2007). Improved modeling of fission-track annealing in apatite. *American Mineralogist*, 92(5–6), 799–810. <https://doi.org/10.2138/am.2007.2281>
- Ketcham, R. A., Gautheron, C., & Tassan-Got, L. (2011). Accounting for long alpha-particle stopping distances in (U–Th–Sm)/He geochronology: Refinement of the baseline case. *Geochimica et Cosmochimica Acta*, 75(24), 7779–7791. <https://doi.org/10.1016/j.gca.2011.10.011>
- Kirchner, K. L., Behr, W. M., Loewy, S., & Stockli, D. F. (2016). Early Miocene subduction in the western Mediterranean: Constraints from Rb–Sr multimineral isochron geochronology. *Geochemistry, Geophysics, Geosystems*, 17, 1842–1860. <https://doi.org/10.1002/2015GC006208>
- Labails, C., Olivet, J. L., Aslanian, D., & Roest, W. R. (2010). An alternative early opening scenario for the Central Atlantic Ocean. *Earth and Planetary Science Letters*, 297(3–4), 355–368. <https://doi.org/10.1016/j.epsl.2010.06.024>
- Leprêtre, R., de Lamotte, D. F., Combier, V., Gimeno-Vives, O., Mohn, G., & Eschard, R. (2018). The Tell-Rif orogenic system (Morocco, Algeria, Tunisia) and the structural heritage of the southern Tethys margin. *BSGF-Earth Sciences Bulletin*, 189(2), 10. <https://doi.org/10.1051/bsgf/2018009>
- Li, B., & Massonne, H. J. (2018). Two Tertiary metamorphic events recognized in high-pressure metapelites of the Nevado-Filabride Complex (Betic Cordillera, S Spain). *Journal of Metamorphic Geology*, 36(5), 603–630. <https://doi.org/10.1111/jmg.12312>
- Lonergan, L. (1993). Timing and kinematics of deformation in the Malaguide Complex, internal zone of the Betic Cordillera, Southeast Spain. *Tectonics*, 12(2), 460–476. <https://doi.org/10.1029/92TC02507>
- Lonergan, L., & Johnson, C. (1998). Reconstructing orogenic exhumation histories using synorogenic detrital zircons and apatites: An example from the Betic Cordillera, SE Spain. *Basin Research*, 10(3), 353–364. <https://doi.org/10.1046/j.1365-2117.1998.00071.x>
- Lonergan, L., & Mange-Rajetzyk, M. A. (1994). Evidence for Internal Zone unroofing from foreland basin sediments, Betic Cordillera, SE Spain. *Journal of the Geological Society*, 151(3), 515–529. <https://doi.org/10.1144/gsjgs.151.3.0515>
- Lonergan, L., & White, N. (1997). Origin of the Betic-Rif mountain belt. *Tectonics*, 16(3), 504–522. <https://doi.org/10.1029/96TC03937>
- López-Gómez, J., Alonso-Azcárate, J., Arche, A., Arribas, J., Fernández Barrenechea, J., Borruel-Abadía, V., et al. (2019). Permian-Triassic rifting stage. In C. Quesada, & J. Oliveira (Eds.), *The Geology of Iberia: A Geodynamic Approach* (pp. 29–112). Cham: Regional Geology Reviews. Springer.
- Luján, M., Crespo-Blanc, A., & Balanyá, J. C. (2006). The Flysch Trough thrust imbricate (Betic Cordillera): A key element of the Gibraltar Arc orogenic wedge. *Tectonics*, 25, TC6001. <https://doi.org/10.1029/2005TC001910>
- Maaté, A., Martín-Algarra, A., Martín-Martín, M., & Serra-Kiel, J. (2000). Nouvelles données sur le Paléocène-Éocène des zones internes bético-rifaines. *Geobios*, 33(4), 409–418. [https://doi.org/10.1016/S0016-6995\(00\)80074-1](https://doi.org/10.1016/S0016-6995(00)80074-1)
- Macchiavelli, C., Vergés, J., Schettino, A., Fernández, M., Turco, E., Casciello, E., et al. (2017). A new southern North Atlantic Isochron map: Insights into the drift of the Iberian plate since the late Cretaceous. *Journal of Geophysical Research: Solid Earth*, 122, 9603–9626. <https://doi.org/10.1002/2017JB014769>
- Mancilla, F. L., Booth-Rea, G., Stich, D., Pérez-Peña, J. V., Morales, J., Azañón, J. M., et al. (2015). Slab rupture and delamination under the Betics and Rif constrained from receiver functions. *Tectonophysics*, 663, 225–237. <https://doi.org/10.1016/j.tecto.2015.06.028>
- Martín-Algarra, A. (1987). *Evolución geológica alpina del contacto entre las Zonas Internas y las Zonas Externas de la Cordillera Bética - Thesis* (p. 1171). Univ. Granada.
- Martín-Algarra, A., Mazzoli, S., Perrone, V., Rodríguez-Cañero, R., & Navas-Parejo, P. (2009). Variscan tectonics in the Malaguide Complex (Betic Cordillera, southern Spain): Stratigraphic and structural Alpine versus pre-Alpine constraints from the Ardales area (province of Málaga) I. Stratigraphy. *The Journal of Geology*, 117(3), 241–262. <https://doi.org/10.1086/597364>
- Martín-Chivelet, J., Berástegui, X., Rosales, I., Vilas, L., Vera, J. A., Caus, E., & Robles, S. (2002). Cretaceous. In *The Geology of Spain* (pp. 255–292). Geological Society of London. <https://doi.org/10.1144/GOSPP.12>
- Martín-Chivelet, J., & Chacón, B. (2007). Event stratigraphy of the upper Cretaceous to lower Eocene hemipelagic sequences of the Prebetic Zone (SE Spain): Record of the onset of tectonic convergence in a passive continental margin. *Sedimentary Geology*, 197(1–2), 141–163. <https://doi.org/10.1016/j.sedgeo.2006.09.007>
- Martínez-Martínez, J., Soto, J., & Balanyá, J. (2002). Orthogonal folding of extensional detachments: Structure and origin of the Sierra Nevada elongated dome (Betics, SE Spain). *Tectonics*, 21(3), 3–1–3–20. <https://doi.org/10.1029/2001tc001283>
- Martín-Martín, M. (1996). *El Terciario del Dominio Malagueño en Sierra Espuña (Cordillera Bética oriental. SE de España)*, Tesis (p. 299). Univ. Granada, Publ. Dpto. Estratigrafía y Paleontología.
- Martínez-García, P., Comas, M., Lonergan, L., & Watts, A. B. (2017). From extension to shortening: Tectonic inversion distributed in time and space in the Alboran Sea, western Mediterranean. *Tectonics*, 36, 2777–2805. <https://doi.org/10.1002/2017TC004489>

- Mesalles, L., Mouthereau, F., Bernet, M., Chang, C. P., Tien-Shun Lin, A., Fillon, C., & Sengelen, X. (2014). From submarine continental accretion to arc-continent orogenic evolution: The thermal record in southern Taiwan. *Geology*, 42(10), 907–910. <https://doi.org/10.1130/G35854.1>
- Michard, A., Feinberg, H., El-Azzab, D., Bouybaouene, M., & Saddiqi, O. (1992). A serpentinite ridge in a collisional paleomargin setting: The Beni Malek massif, external Rif, Morocco. *Earth and Planetary Science Letters*, 113(3), 435–442. [https://doi.org/10.1016/0012-821X\(92\)90144-K](https://doi.org/10.1016/0012-821X(92)90144-K)
- Michard, A., Saddiqi, O., Chalouan, A., & de Lamotte, D. F. (2008). *Continental evolution: The Geology of Morocco: Structure, Stratigraphy, and Tectonics of the Africa-Atlantic-Mediterranean Triple Junction* (Vol. 116). Berlin Heidelberg: Springer. <https://doi.org/10.1007/978-3-540-77076-3>
- Moni, P., Galindo-Zaldívar, J., Lodeiro, F. G., Goffe, B., & Jabaloy, A. (1991). 40Ar/39Ar geochronology of Alpine tectonism in the Betic Cordilleras (southern Spain). *Journal of the Geological Society*, 148(2), 289–297. <https://doi.org/10.1144/gsjgs.148.2.0289>
- Monié, P., Torres-Roldán, R., & García-Casco, A. (1994). Cooling and exhumation of the Western Betic Cordilleras, 40Ar/39Ar thermochronological constraints on a collapsed terrane. *Tectonophysics*, 238(1-4), 353–379. [https://doi.org/10.1016/0040-1951\(94\)90064-7](https://doi.org/10.1016/0040-1951(94)90064-7)
- Mouthereau, F., Filleaudeau, P. Y., Vacherat, A., Pik, R., Lacombe, O., Fellin, M. G., et al. (2014). Placing limits to shortening evolution in the Pyrenees: Role of margin architecture and implications for the Iberia/Europe convergence. *Tectonics*, 33, 2283–2314. <https://doi.org/10.1002/2014TC003663>
- Müller, R., Seton, M., Zahirovic, S., Williams, S., Matthews, K., Wright, N., et al. (2016). Ocean Basin Evolution and Global-Scale Plate Reorganization Events Since Pangea Breakup. *Annual Review of Earth and Planetary Sciences*, 44(1), 107–138. <https://doi.org/10.1146/annurev-earth-060115-012211>
- Murray, K. E., Orme, D. A., & Reiners, P. W. (2014). Effects of U-Th-rich grain boundary phases on apatite helium ages. *Chemical Geology*, 390, 135–151. <https://doi.org/10.1016/j.chemgeo.2014.09.023>
- Nirrengarten, M., Manatschal, G., Tugend, J., Kusznir, N., & Sauter, D. (2018). Kinematic evolution of the southern North Atlantic: Implications for the formation of hyperextended rift systems. *Tectonics*, 37, 89–118. <https://doi.org/10.1002/2017TC004495>
- O'Sullivan, P. B., & Parrish, R. R. (1995). The importance of apatite composition and single-grain ages when interpreting fission track data from plutonic rocks: A case study from the Coast Ranges, British Columbia. *Earth and Planetary Science Letters*, 132(1–4), 213–224. [https://doi.org/10.1016/0012-821x\(95\)00058-k](https://doi.org/10.1016/0012-821x(95)00058-k)
- Olivier, P. (1984). *Évolution de la limite entre zones internes et zones externes dans l'arc de Gibraltar (Maroc, Espagne)*, thèse (Vol. 3, p. 229). Université Toulouse.
- Orti, F., Pérez-López, A., & Salvany, J. M. (2017). Triassic evaporites of Iberia: Sedimentological and palaeogeographical implications for the western Neotethys evolution during the Middle Triassic-Earliest Jurassic. *Palaeogeography, Palaeoclimatology, Palaeoecology*, 471, 157–180. <https://doi.org/10.1016/j.palaeo.2017.01.025>
- Palomeras, I., Villaseñor, A., Thurner, S., Levander, A., Gallart, J., & Harnafi, M. (2017). Lithospheric structure of Iberia and Morocco using finite-frequency Rayleigh wave tomography from earthquakes and seismic ambient noise. *Geochemistry, Geophysics, Geosystems*, 18, 1824–1840. <https://doi.org/10.1002/2016GC006657>
- Pérez-Valera, F., Sánchez-Gómez, M., Pérez-López, A., & Pérez-Valera, L. (2017). An evaporite-bearing accretionary complex in the northern front of the Betic-Rif orogen. *Tectonics*, 36, 1006–1036. <https://doi.org/10.1002/2016TC004414>
- Perri, F., Critelli, S., Martín-Algarra, A., Martín-Martín, M., Perrone, V., Mongelli, G., & Zattin, M. (2013). Triassic redbeds in the Malaguide Complex (Betic Cordillera—Spain): Petrography, geochemistry and geodynamic implications. *Earth-Science Reviews*, 117, 1–28. <https://doi.org/10.1016/j.earscirev.2012.11.002>
- Petit, C., Le Pourtier, L., Scalabrino, B., Corsini, M., Bonnin, M., & Romagny, A. (2015). Crustal structure and gravity anomalies beneath the Rif, northern Morocco: Implications for the current tectonics of the Alboran region. *Geophysical Journal International*, 202(1), 640–652. <https://doi.org/10.1093/gji/ggv169>
- Peyre, Y. (1974). *Géologie d'Antequera et de sa région (Cordillères bétiques-Espagne)*. Paris: Université de Paris, Institut National Agronomique Paris.
- Platt, J. P., Allerton, S., Kirker, A., Mandeville, C., Mayfield, A., Platzman, E. S., & Rimi, A. (2003). The ultimate arc: Differential displacement, oroclinal bending, and vertical axis rotation in the External Betic-Rif arc. *Tectonics*, 22(3), 1017. <https://doi.org/10.1029/2001TC001321>
- Platt, J. P., Anczkiewicz, R., Soto, J. I., Kelley, S. P., & Thirlwall, M. (2006). Early Miocene continental subduction and rapid exhumation in the western Mediterranean. *Geology*, 34(11), 981–984. <https://doi.org/10.1130/g22801a.1>
- Platt, J. P., Argles, T. W., Carter, A., Kelley, S. P., Whitehouse, M. J., & Lonergan, L. (2003). Exhumation of the Ronda peridotite and its crustal envelope: Constraints from thermal modelling of a P-T-time array. *Journal of the Geological Society*, 160(5), 655–676. <https://doi.org/10.1144/0016-764902-108>
- Platt, J. P., Behr, W. M., Johanesen, K., & Williams, J. R. (2013). The Betic-Rif arc and its orogenic hinterland: A review. *Annual Review of Earth and Planetary Sciences*, 41, 313–357. <https://doi.org/10.1146/annurev-earth-050212-123951>
- Platt, J. P., Kelley, S. P., Carter, A., & Orozco, M. (2005). Timing of tectonic events in the Alpujarride Complex, Betic Cordillera, southern Spain. *Journal of the Geological Society*, 162(3), 451–462. <https://doi.org/10.1144/0016-764903-039>
- Platt, J. P., & Vissers, R. L. M. (1989). Extensional collapse of thickened continental lithosphere: A working hypothesis for the Alboran Sea and Gibraltar arc. *Geology*, 17(6), 540–543. [https://doi.org/10.1130/0091-7613\(1989\)017<0540:ecotcl>2.3.co;2](https://doi.org/10.1130/0091-7613(1989)017<0540:ecotcl>2.3.co;2)
- Platt, J., Whitehouse, M., Kelley, S., Carter, A., & Hollick, L. (2003). Simultaneous extensional exhumation across the Alboran Basin: Implications for the causes of late orogenic extension. *Geology*, 31(3), 251–254. [https://doi.org/10.1130/0091-7613\(2003\)031<0251:seata>2.0.co;2](https://doi.org/10.1130/0091-7613(2003)031<0251:seata>2.0.co;2)
- Puga, E., De Federico, A. D., & Nieto, J. M. (2002). Tectonostratigraphic subdivision and petrological characterisation of the deepest complexes of the Betic zone: a review. *Geodinamica Acta*, 15(1), 23–43. <https://doi.org/10.1080/09853111.2002.10510737>
- Ramos, A., Fernández, O., Terrinha, P., & Muñoz, J. A. (2016). Extension and inversion structures in the Tethys-Atlantic linkage zone, Algarve Basin, Portugal. *International Journal of Earth Sciences*, 105(5), 1663–1679. <https://doi.org/10.1007/s00531-015-1280-1>
- Ramos, A., Fernández, O., Terrinha, P., & Muñoz, J. A. (2017). Neogene to recent contraction and basin inversion along the Nubia-Iberia boundary in SW Iberia. *Tectonics*, 36, 257–286. <https://doi.org/10.1002/2016TC004262>
- Rat, J., Mouthereau, F., Brichau, S., Crémades, A., Bernet, M., Balvay, M., et al. (2019). Tectonothermal Evolution of the Cameros Basin: Implications for Tectonics of North Iberia. *Tectonics*, 40(3), 327. <https://doi.org/10.1029/2018tc005294>
- Recanati, A., Missenard, Y., Leprêtre, R., Gautheron, C., Barbarand, J., Abbassene, F., et al. (2019). A Tortonian onset for the Algerian margin inversion: Evidence from low-temperature thermochronology. *Terra Nova*, 31(1), 39–48. <https://doi.org/10.1111/ter.12367>

- Rosenbaum, G., Lister, G. S., & Duboz, C. (2002). Reconstruction of the tectonic evolution of the western Mediterranean since the Oligocene. *Journal of the Virtual Explorer*, 8, 107–130. <https://doi.org/10.3809/jvirtex.2002.00053>
- Roure, F., Casero, P., & Addoum, B. (2012). Alpine inversion of the North African margin and delamination of its continental lithosphere. *Tectonics*, 31. <https://doi.org/10.1029/2011tc002989>
- Sánchez-Navas, A., García-Casco, A., & Martín-Algarra, A. (2014). Pre-Alpine discordant granitic dikes in the metamorphic core of the Betic Cordillera: Tectonic implications. *Terra Nova*, 26(6), 477–486. <https://doi.org/10.1111/ter.12123>
- Sánchez-Navas, A., García-Casco, A., Mazzoli, S., & Martín-Algarra, A. (2017). Polymetamorphism in the Alpujarride Complex, Betic Cordillera, South Spain. *The Journal of Geology*, 125(6), 637–657. <https://doi.org/10.1086/693862>
- Sánchez-Rodríguez, L., & Gebauer, D. (2000). Mesozoic formation of pyroxenites and gabbros in the Ronda area (southern Spain), followed by Early Miocene subduction metamorphism and emplacement into the middle crust: U–Pb sensitive high-resolution ion microprobe dating of zircon. *Tectonophysics*, 316(1–2), 19–44. [https://doi.org/10.1016/s0040-1951\(99\)00256-5](https://doi.org/10.1016/s0040-1951(99)00256-5)
- Sánchez-Vizcaíno, V., Rubatto, D., Gómez-Pugnaire, M., Trommsdorff, V., & Müntener, O. (2001). Middle Miocene high-pressure metamorphism and fast exhumation of the Nevado-Filábride Complex, SE Spain: Fast cooling and exhumation of the Nevado-Filábride. *Terra Nova*, 13(5), 327–332. <https://doi.org/10.1046/j.1365-3121.2001.00354.x>
- Sehrt, M., Glasmacher, U., Stockli, D., Jabour, H., & Kluth, O. (2018). The southern Moroccan passive continental margin: An example of differentiated long-term landscape evolution in Gondwana. *Gondwana Research*, 53, 129–144. <https://doi.org/10.1016/j.gr.2017.03.013>
- Serra-Kiel, J., Martín-Martín, M., El Mamoune, B., Martín-Algarra, A., Tosquella, I., Angrill, J., & Serrano, F. (1998). Bioestratigrafía y litoestratigrafía del Paleógeno del área de Sierra Espuña (Cordillera Bética oriental, SE de España). *Acta Geológica Hispánica*, 31, 161–182.
- Serrano, F., Guerra-Merchán, A., El Kadiri, K., de Galdeano, C. S., López-Garrido, Á. C., Martín-Martín, M., & Hlila, R. (2007). Tectono-sedimentary setting of the Oligocene-early Miocene deposits on the Betic-Rifian Internal Zone (Spain and Morocco). *Geobios*, 40(2), 191–205.
- Serrano, F., Sanz de Galdeano, C., Delgado, F., López-Garrido, A. C., & Martín-Algarra, A. (1995). The Mesozoic and Cenozoic of the Malaguide Complex in the Málaga area: A Paleogene olistostrome-type chaotic complex (Betic Cordillera, Spain). *Geologie en Mijnbouw*, 74, 105–105.
- Sosson, M., Morrillon, A. C., Bourgois, J., Féraud, G., Poupeau, G., & Saint-Marc, P. (1998). Late exhumation stages of the Alpujarride Complex (western Betic Cordilleras, Spain): New thermochronological and structural data on Los Reales and Ojen nappes. *Tectonophysics*, 285(3–4), 253–273. [https://doi.org/10.1016/s0040-1951\(97\)00274-6](https://doi.org/10.1016/s0040-1951(97)00274-6)
- Spakman, W., & Wortel, R. (2004). A tomographic view on western Mediterranean geodynamics. In *The TRANSMED atlas. The Mediterranean region from crust to mantle* (pp. 31–52). Berlin, Heidelberg: Springer.
- Spiegel, C., Kohn, B., Belton, D., Berner, Z., & Gleadow, A. (2009). Apatite (U-Th-Sm)/He thermochronology of rapidly cooled samples: The effect of He implantation. *Earth and Planetary Science Letters*, 285, 105–114. <https://doi.org/10.1016/j.epsl.2009.05.045>
- Suades, E., & Crespo-Blanc, A. C. (2013). Gravitational dismantling of the Miocene mountain front of the Gibraltar Arc system deduced from the analysis of an olistostromic complex (western Betics). *Geologica Acta: an international earth science journal*, 11(2), 215–229.
- Thurner, S., Palomeras, I., Levander, A., Carbonell, R., & Lee, C. T. (2014). Ongoing lithospheric removal in the western Mediterranean: Evidence from Ps receiver functions and thermobarometry of Neogene basalts (PICASSO project). *Geochemistry, Geophysics, Geosystems*, 15, 1113–1127. <https://doi.org/10.1002/2013GC005124>
- Tubia, J. M., Cuevas, J., Esteban, J. J., & Gil Ibarguchi, J. I. (2009). Remnants of a Mesozoic rift in a subducted terrane of the Alpujarride Complex (Betic Cordilleras, southern Spain). *The Journal of Geology*, 117(1), 71–87. <https://doi.org/10.1086/593322>
- Vacherat, A., Moutherieu, F., Pik, R., Bernet, M., Gautheron, C., Masini, E., et al. (2014). Thermal imprint of rift-related processes in orogens as recorded in the Pyrenees. *Earth and Planetary Science Letters*, 408, 296–306. <https://doi.org/10.1016/j.epsl.2014.10.014>
- van Hinsbergen, D. J., Vissers, R. L., & Spakman, W. (2014). Origin and consequences of western Mediterranean subduction, rollback, and slab segmentation. *Tectonics*, 33, 393–419. <https://doi.org/10.1002/2013TC003349>
- Vázquez, M., Jabaloy, A., Barbero, L., & Stuart, F. M. (2011). Deciphering tectonic-and erosion-driven exhumation of the Nevado-Filábride Complex (Betic Cordillera, Southern Spain) by low temperature thermochronology. *Terra Nova*, 23(4), 257–263. <https://doi.org/10.1111/j.1365-3121.2011.01007.x>
- Vera, J. A. (2000). El Terciario de la Cordillera Bética: estado actual de conocimientos. *Revista de la Sociedad Geológica de España*, 13(2), 345–373.
- Vera, J. A., Arias, C., García-Hernández, M., López-Garrido, A. C., Martín-Algarra, A., Martín-Chivelet, J., et al. (2004). Las zonas externas Béticas y el paleomargin Sudibérico. *J. A. Vera Geología de España, Sociedad Geológica de España* (pp. 354–361).
- Vergés, J., & Fernández, M. (2012). Tethys–Atlantic interaction along the Iberia–Africa plate boundary: The Betic–Rif orogenic system. *Tectonophysics*, 579, 144–172. <https://doi.org/10.1016/j.tecto.2012.08.032>
- Vermeesch, P. (2009). RadialPlotter: A Java application for fission track, luminescence and other radial plots. *Radiation Measurements*, 44(4), 409–410. <https://doi.org/10.1016/j.radmeas.2009.05.003>
- Vernant, P., Fadil, A., Mourabit, T., Ouazar, D., Koulali, A., Davila, J., et al. (2010). Geodetic constraints on active tectonics of the Western Mediterranean: Implications for the kinematics and dynamics of the Nubia-Eurasia plate boundary zone. *Journal of Geodynamics*, 49(3–4), 123–129. <https://doi.org/10.1016/j.jog.2009.10.007>
- Villaseñor, A., Chevrot, S., Harnafi, M., Gallart, J., Pazos, A., Serrano, I., et al. (2015). Subduction and volcanism in the Iberia–North Africa collision zone from tomographic images of the upper mantle. *Tectonophysics*, 663, 238–249. <https://doi.org/10.1016/j.tecto.2015.08.042>
- Vissers, R. L. M., Platt, J. P., & Van der Wal, D. (1995). Late orogenic extension of the Betic Cordillera and the Alboran Domain: A lithospheric view. *Tectonics*, 14(4), 786–803. <https://doi.org/10.1029/95TC00086>
- Wildi, W. (1983). La chaîne tello-rifaïne (Algérie, Maroc, Tunisie): Structure, stratigraphie et évolution du Trias au Miocène. *Revue de Géographie Physique et de Géologie Dynamique*, 24(3), 201–297.
- Zeck, H. P., Monié, P., Villa, I. M., & Hansen, B. T. (1992). Very high rates of cooling and uplift in the Alpine belt of the Betic Cordilleras, southern Spain. *Geology*, 20(1), 79–82. [https://doi.org/10.1130/0091-7613\(1992\)020<0079:vhroca>2.3.co;2](https://doi.org/10.1130/0091-7613(1992)020<0079:vhroca>2.3.co;2)
- Zeck, H. P., & Whitehouse, M. J. (2002). Repeated age resetting in zircons from Hercynian–Alpine polymetamorphic schists (Betic–Rif tectonic belt, S. Spain)—a U–Th–Pb ion microprobe study. *Chemical Geology*, 182(2–4), 275–292. [https://doi.org/10.1016/s0009-2541\(01\)00296-0](https://doi.org/10.1016/s0009-2541(01)00296-0)